

OPTOELECTRONIC INTEGRATED CIRCUITS

5.1 Introduction

- The display devices and sensors are active components used in information handling systems.
- These includes optical communication systems and computing systems. It is perhaps to examine the role of photonics and electronics.
- Optics provides the inherent advantages to large bandwidth, parallelism and reconfigurable configurations.
- But optics does not provide input-output isolation, as electronic devices do and it can be difficult to focus multiple beams in a parallel system. Therefore to couple electronic and photonic devices, resulting in “**optoelectronic Integration**”.
- Opto-Electronic Integration is a technology that combines optical component with the photonic components on a single wafer to obtain highly functional circuit.
- It is known, both optical communication systems and computing systems is the interconnect medium.
- The performance of conventional electrical inter connects is adversely affected by increases in reactance and reflections due to impedance mismatch at the higher frequencies.
- Multi level board technology is being developed i.e. chip-to-chip communication is achieved through via-holes in the wafers.

- Even these fail to perform as operating frequencies approach the gigahertz range.
- An attractive and alternative method is an optical inter connect medium , which can take the form of free space, integrated optical waveguides (or) optical fibers.
- Optical interconnects and transmission media provide, **large band width** and **high speed data transmission**.
- It is immunity to **mutual interference** and **cross talk** and freedom from capacitive loading effects.
- Large bandwidth translates
 - reduced system size
 - reduced system power
 - increased fanout capabilities
- Optoelectronic integrated circuits (OEIC) involve the integration of electronic and optical components.

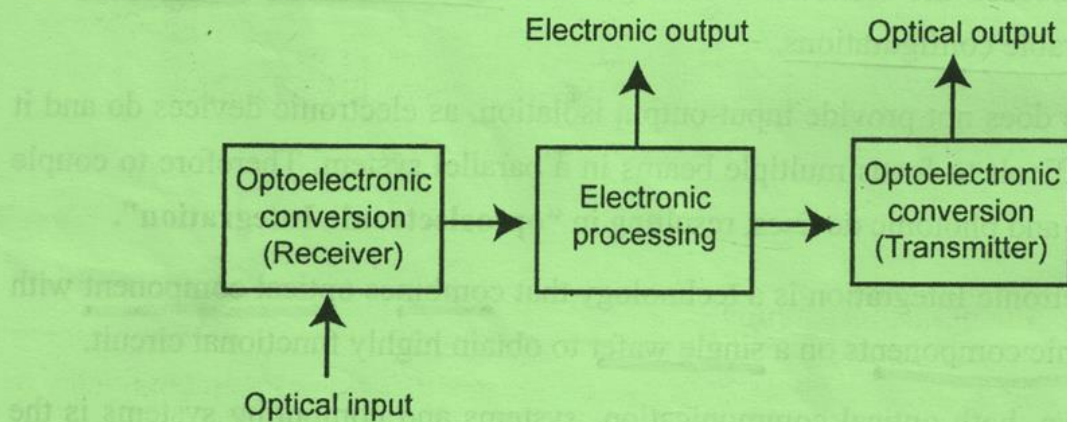


Figure 5.1 Block diagram of essential elements of an OEIC

- The monolithic integration of electronic and optical devices on the same chip will give the following advantages.
 - high speed**
 - high sensitivity**

(iii) compactness

(iv) reliability

(v) low cost

Lay out of optical fiber link

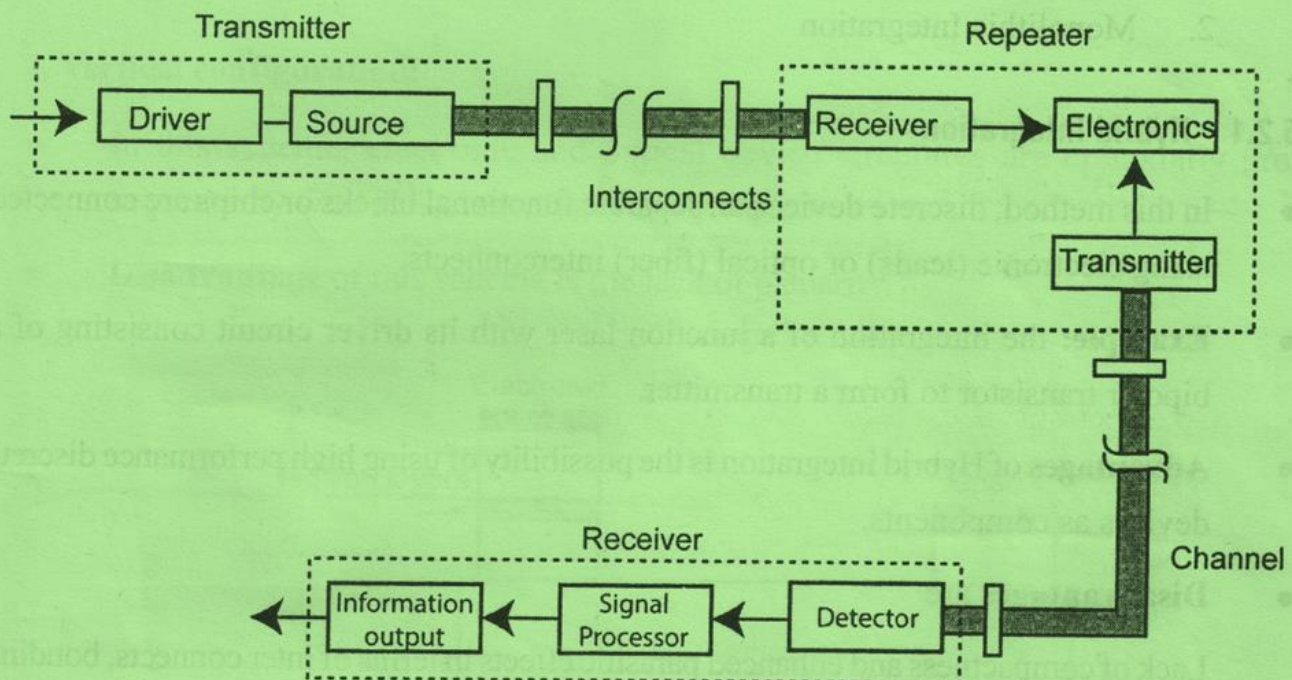


Figure 5.2

5.2 Hybrid and Monolithic Integration

- Electrons and photons interact effectively in a direct bandgap semiconductor to produce opto-electronic conversion.
- An optoelectronic device is a good example of collaborative role of electrons and photons to perform a single function either emission or detection.
- An optoelectronic system in which multiple functions are separately performed by electronic and optoelectronic devices. Such a system by analogy with the integrated circuit (IC) can be called as '**optoelectronic Integrated circuits**' (OEIC).
- Electronic functions such as switching or amplification can be combined with detection and also light transmission in integrated chip.

- Need for Integration arises from a variety of needs, such as speed and bandwidth, functionality and multifunction capabilities, compactness, low parasitics, etc.
- OEIC will play a pivotal role in the development of future optoelectronic systems.
- There are two types of optoelectronic integration.
 1. Hybrid integration
 2. Monolithic Integration

5.2.1 Hybrid Integration

- In this method, discrete devices on separate functional blocks or chips are connected using electronic (leads) or optical (fiber) interconnects.
- **Example:** the integration of a junction laser with its driver circuit consisting of a bipolar transistor to form a transmitter.
- **Advantages** of Hybrid integration is the possibility of using high performance discrete devices as components.
- **Disadvantages** are

Lack of compactness and enhanced parasitic effects in terms of inter connects, bonding and lead wires.

- Parasitic are considerably reduced in “flip-chip” bonding, in which two chips containing component devices and circuits are interconnected by indium bumps.

5.2.2 Monolithic Integration

- In this all active and passive components are fabricated on the same chip. All parts are made with same materials and same processing steps, the hetero structures and processing steps of the different components of a OEIC can be different. This makes the realization of high performance monolithic OEICs a real challenge.
- **Advantages** are size reduction, reduction of parasitic and the consequent achievements of higher-circuit speed and bandwidth.

- Monolithic Integration can be achieved by two ways

- Vertical configuration
- Horizontal configuration
 - Planar compatible
 - Planar regrown

1. Vertical configuration:

- In this scheme, electronic and optical device structures are epitaxially grown sequentially with an isolation layer in between
- Disadvantage** of this scheme is the lack of planarity.

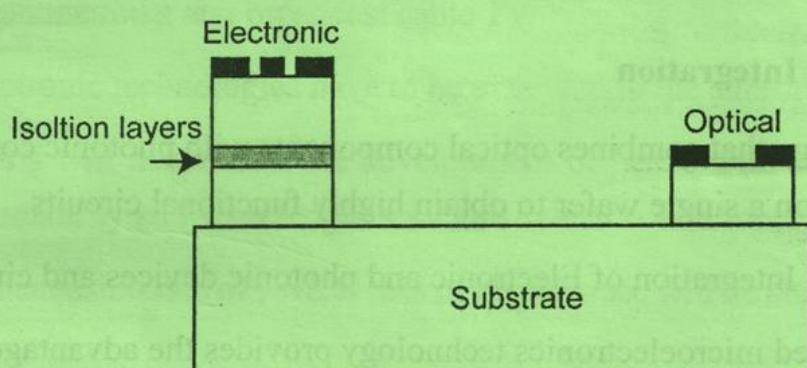


Figure 5.3 Schematic diagram of vertical Integration

2. Horizontal Configuration:

(i) Planar compatible:

- Electronic and optical devices are made from the same hetero structure

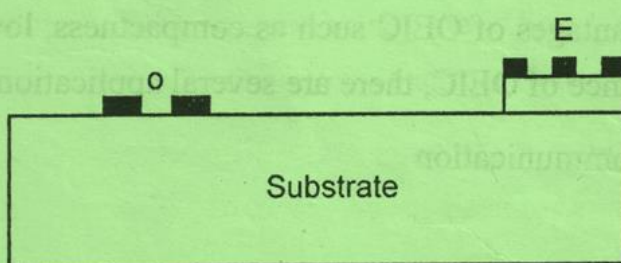


Figure 5.4 Planar-compatible scheme

- This technique provides a large freedom in the choice of device hetero structures, the regrown interface can have a large density of traps and other electrically active defects that can affect the performance of the regrown device.

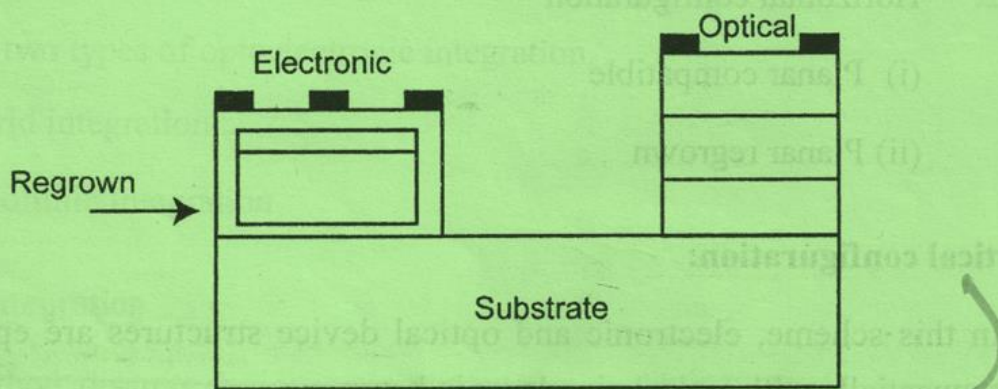


Figure 5.5 Planar regrown scheme

5.3. Applications of opto Electronic Integrated Circuits

Opto-Electronic Integration

- A technology that combines optical components with photonic components such as transistors on a single wafer to obtain highly functional circuits.
ie.OEIC → Integration of Electronic and photonic devices and circuits
- Silicon based microelectronics technology provides the advantages of
 - Low cost
 - Large scale integration and
 - Ruggedness
- Photonic devices and circuits can serve unique functions that are complementary of electronic devices.
- Based on the advantages of OEIC such as compactness, low cost, ruggedness and superior performance of OEIC, there are several applications.
 - Telecommunication
 - Radar
 - Local Area Network

- (iv) Intelligent sensors
- (v) Fiber transceivers
- (vi) Smart pixel arrays
- (vii) Diffuse optical tomography
- (viii) Optical computing systems

5.3.1 Telecommunications Applications

- One of the primary areas where OEICs will make an impact is telecommunication
- Telecommunication has large bandwidth and light weight of optical fibres.
- The object is to bring the fiber systems to the home and individual subscribers in the form of telephone links and broadcast cable TV.
- The optoelectronic technologies have to be extended to the subscriber loop.
- These systems will necessitate the development of lasers with precise frequency control and tunability and wavelength selective detectors and receivers.
- The data transmission rate of several tens of gigabits/sec will be attained using these circuits.

9.4

Integrated optics

Although signal transmission using light waves is now well established, the optical signal usually has to be converted back into an electrical one if any processing needs to be done. The aim of integrated optics (IO) is to be able to carry out as much signal processing as possible on the optical signal itself. It is envisaged that a family of optical and electro-optical elements in thin film planar form will be used, allowing the assembly of a large number of such devices on a single substrate. Most device elements are expected to be based on single mode planar optical waveguides. Similar advantages are expected to those accruing when the idea of the integrated circuit was adopted in electronics.

The basic concept of IO was first proposed by Anderson in 1965 (ref. 9.14) and considerable progress has been made since then. (For a fairly comprehensive coverage of the field, the reader may consult ref. 9.15.) Initially most effort was put into demonstrating the viability of a wide range of individual devices, whilst latterly interest has concentrated on the problem of device integration. One of the main difficulties has been that no one substrate is ideally suited for all the different types of device. Many of the earlier composite devices were based on hybrid structures (see e.g. Fig. 9.48) but recently more fully integrated structures have begun to emerge.

9.4.1 Slab and stripe waveguides

It is generally assumed that in IO the signal will be carried within planar waveguides in either slab or stripe form which are formed by modifying the surface of a substrate. Planar waveguides were discussed in section 8.2, but there we confined our attention to symmetrical guides. In the present instance we are usually dealing with *asymmetrical* guides, that is guides where the layers above and below the guiding layer have different refractive indices (Fig. 9.33). The topmost layer (of refractive index n_0) is often air and consequently has a much lower refractive index than either the guide layer (n_1) or the substrate (n_2); such a guide is

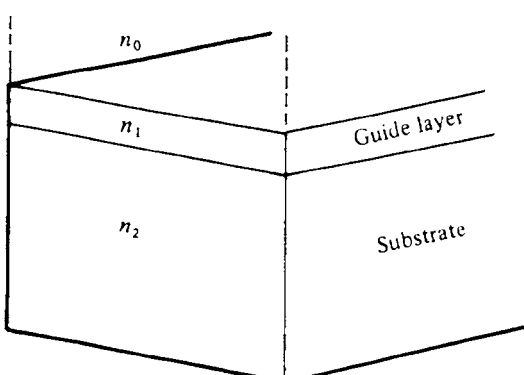


FIG. 9.33 Slab planar waveguide. The guide itself is formed on a substrate. The medium above the guide is usually air. The refractive indices of substrate, guide and topmost layer are n_2 , n_1 and n_0 respectively.

thus referred to as a *strongly asymmetric* guide. It is a relatively simple matter to extend the treatment of symmetric guides given in section 8.2 to cover the strongly asymmetric case.

We suppose that the phase changes at the upper and lower interfaces are $\phi_1(\theta)$ and $\phi_2(\theta)$ respectively, and using similar arguments that led up to eq. (8.9) the condition for a ray to be able to propagate becomes

$$\frac{4\pi n_1 d \cos \theta}{\lambda_0} - \phi_1(\theta) - \phi_2(\theta) = 2m\pi$$

For a ray to undergo total internal reflection at both the upper and lower interfaces, the internal guide angle must always be greater than either of the critical angles of the upper and lower interfaces (denoted by θ_{c1} and θ_{c2} respectively). Because we have a strongly asymmetric guide the critical angle at the upper interface will be much smaller than that at the lower. Thus as far as guided rays are concerned, we can assume that the internal guide angle will always be much larger than the critical angle of the lower interface, and consequently we may approximate $\phi_1(\theta)$ by π . The propagation condition can now be written

$$\frac{4\pi n_1 d \cos \theta}{\lambda_0} = \phi_2(\theta) + (2m + 1)\pi \quad (9.23)$$

Following a similar line of reasoning that led up to eq. (8.12), the condition for the $m = 1$ mode to propagate becomes

$$\frac{4\pi n_1 d \cos \theta_{c2}}{\lambda_0} > 3\pi$$

In contrast to the symmetric waveguide case, it is now possible for no mode at all to propagate, which happens when

$$\frac{4\pi n_1 d \cos \theta_{c2}}{\lambda_0} < \pi$$

Thus the condition for only a single mode to propagate now becomes

$$\pi \leq \frac{4\pi n_1 d \cos \theta_{c2}}{\lambda_0} \leq 3\pi$$

By putting $\cos \theta_{c2} = [1 - (n_2/n_1)^2]^{1/2}$ this condition can be written

$$\frac{\pi}{4} \leq V \leq \frac{3\pi}{4} \quad (9.24)$$

where V is as defined in eq. (8.14). In terms of the guide thickness d we have

$$\frac{1}{4(\text{NA})} \leq \frac{d}{\lambda_0} \leq \frac{3}{4(\text{NA})} \quad (9.25)$$

where $\text{NA} = (n_1^2 - n_2^2)^{1/2}$.

This equation implies that, in contrast to the symmetrical guide case, there is a minimum thickness below which it is not possible for the guide to support a single mode. A calculation based on this equation is given in Example 9.3.

EXAMPLE 9.3 Guide thicknesses for strongly asymmetric waveguides

Planar waveguides may be made in LiNbO_3 by diffusing in titanium; a 1% concentration of titanium causes (at a wavelength of $0.63 \mu\text{m}$) a refractive index change of about 6×10^{-3} . The ordinary refractive index of LiNbO_3 is 2.286, so we have $n_1 = 2.286$ and $n_2 = 2.280$ and then $\text{NA} = (2.286^2 - 2.280^2)^{1/2} = 0.166$. Using eq. (9.25) the requirement for single mode behaviour becomes

$$1.51 \leq d/\lambda_0 \leq 6.02$$

The exact value chosen for d/λ_0 depends on the manufacturing process and the use to which the guide is being put. Assuming that it is desirable that the guide be as thick as possible then a suitable design thickness for such a guide could be $d = 5\lambda_0$. It would be unwise to approach the upper limit too closely lest the inevitable fluctuations in d that will occur in any manufacturing process cause the guide to become multimode in some places.

The field distribution can also be derived using a similar approach to that used for the symmetric guide, and is illustrated for a TE_0 -type mode in Fig. 9.34. A cosinusoidal variation is still obtained across the core with the peak being displaced towards the n_2/n_1 interface. Similarly an exponential decline is observed in the cladding but this is now more rapid in the upper medium (n_0) than in the lower (n_2).

The above analysis assumes an infinitely wide waveguide; in practice most waveguides used in IO have an approximately rectangular cross-section so that there is confinement in both the x and y directions. Some typical waveguide configurations are illustrated in Fig. 9.35. A further complication is that the waveguides usually have graded index profiles. There are no general explicit solutions available for either of these situations. A very simplistic

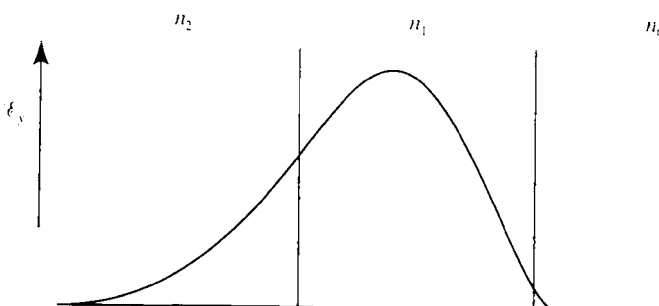


FIG. 9.34 The TE_0 field distribution within a strongly asymmetric planar waveguide, where $n_1 - n_0 \gg n_1 - n_2$.

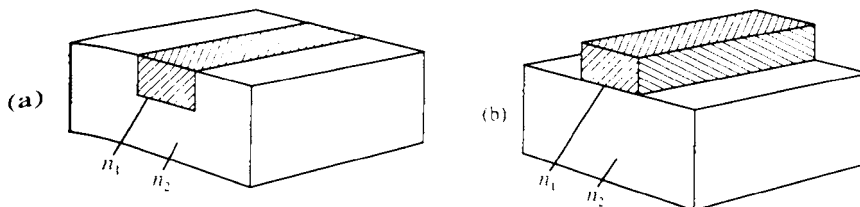


FIG. 9.35 Two basic geometries used for making IO stripe waveguides: (a) the channel waveguide; (b) the ridge waveguide.

view is to assume that, within the waveguide core, the modal field variation with x and y will be given by the product $\mathcal{E}_x(x)\mathcal{E}_y(y)$, where the field $\mathcal{E}_x(x)$ is the solution to the waveguide equation given by assuming the guide is confined in the x direction but unconfined in the y direction (and vice versa for $\mathcal{E}_y(y)$). Such solutions can be useful as the starting point for more accurate 'perturbation'-type calculations, but with the powerful computing facilities now widely available, the field distributions are more readily determined from 'first-principle' calculations involving the point-to-point solution of Maxwell's equations across the guide cross-section.

It is possible to make a few simple generalizations based on our understanding to date. We would expect that in single mode guides the dimensions in both the x and y directions should be of the order of a few times the propagating wavelength (see Example 9.3), and that the mode fields should peak within the core of the guides, declining towards the edges of the core and having a quasi-exponential decline with distance away from the core in the cladding regions.

The three main types of material which have been used as the basis of integrated optical types of waveguides are various types of glass, materials with high electro-optic coefficients such as lithium niobate, and semiconductor materials such as GaAs. A wide variety of different techniques (see ref. 9.16) can be used in waveguide manufacture: examples include sputtering one type of glass onto another, in-diffusion of a layer of titanium deposited on a substrate of lithium niobate, and liquid phase epitaxy. This last technique can be used with semiconducting materials such as GaAs and GaAlAs. The physical extent of the waveguide can often be delineated using the same photo- or electron beam lithography techniques that are common in the semiconductor integrated electronics industry. Losses in IO waveguides are usually much higher than in optical fibers, being of the order of 0.1 dB mm^{-1} . One reason for this is the large scattering from the upper waveguide surface (i.e. the waveguide/air interface) which is often relatively rough. Another problem, which may hinder miniaturization, is that any bends in the waveguides with small radii of curvature (i.e. less than a millimetre or so) must be avoided, otherwise losses can become prohibitively large (see the discussion in section 8.4.1).

9.4.2 Basic IO structural elements

We consider first of all one of the simplest passive devices, a waveguide splitter where an initial single mode waveguide splits into two single mode waveguides of the same width

(Fig. 9.36). In the first section of this device the waveguide expands gradually to twice its original width of a and then the guide splits into two sections each of width a and angled at θ to the original direction. Energy that is in the initial section of the guide will divide itself equally between the two output guides. The loss at the splitting point can be estimated by calculating the overlap integral (eq. 9.9) of the mode field in the section of width $2a$ with the fields in either of the two output sections which are angled at θ to it. An example of such a calculation is given in ref. 9.17; the outcome is that to avoid excessive loss the angle between output waveguides ($= 2\theta$) must be small (usually 1° or less). It should be noted that in this and several subsequent diagrams involving waveguide splitters the angles are shown as being much larger than 0.5° ; this is merely for pictorial convenience.

One of the simplest active devices is a phase modulator which is similar to the Pockels cell discussed in section 3.4. A stripe waveguide is formed within a suitable optically active material such as lithium niobate and electrodes are formed on the substrate surface on either side of the guide (Fig. 9.37). If the electrodes are a distance D apart and extend for a length L , then the additional phase shift $\Delta\phi$ produced when a voltage V is applied across the electrodes is, from eq. (3.14),

$$\Delta\phi = \frac{\pi}{\lambda_0} r n_i^3 V \frac{L}{D} \quad (9.26)$$

where r is the guide material electro-optic coefficient (see Table 3.1 for representative values).

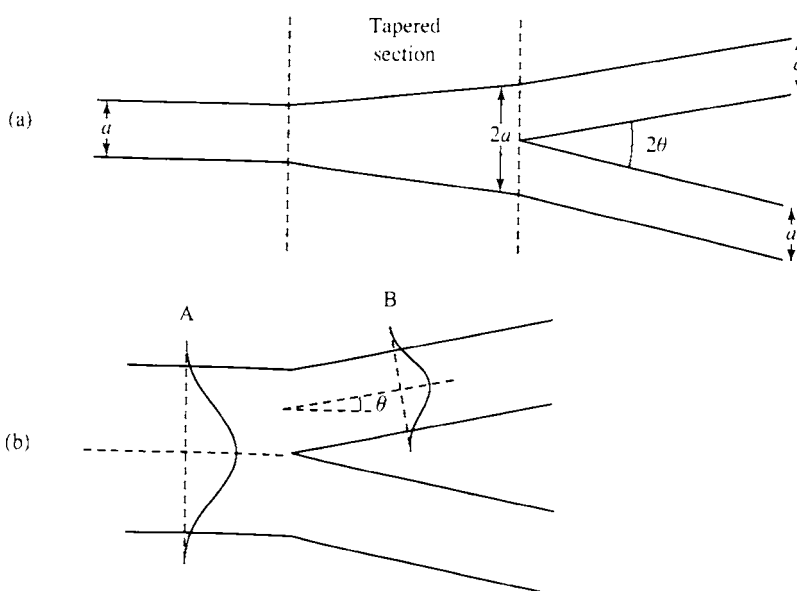


FIG. 9.36 (a) A waveguide 'Y' branch with an angle 2θ between the guides. Before the actual branch point there is a tapered section where the waveguide width is slowly increased from a to $2a$. (b) The efficiency of the splitting process as a function of θ may be calculated by determining the overlap integral of the waveguide modes at points just before (A) and just after (B) the branch point.

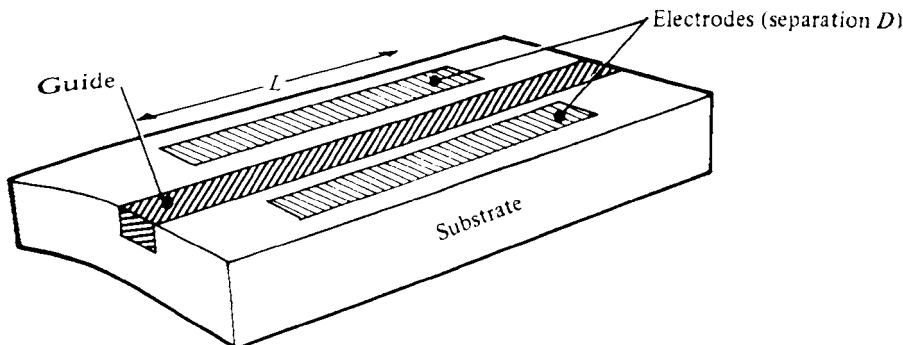


FIG. 9.37 Integrated optical version of the Pockels cell that may be used as a phase shifter.

A big advantage over bulk Pockels effect devices is that the ratio L/D may be made relatively large, say about 1000, and a phase change of π may then be achieved with voltages as low as 1 V or so (see Problem 9.15).

A high speed switch/modulator may be made by incorporating the phase shifter into one arm of the interferometric arrangement shown in Fig. 9.38. This configuration is known as a *Mach-Zehnder* interferometer. In it the guide splits into two with both paths rejoining after an identical path length. With no applied voltage across the phase shifter, the radiation in the two arms will have the same phase when they recombine, and hence the device will not affect the radiation flowing along the guide.³ However, if the phase shifter is activated to give a phase shift of π , then, on recombining, the radiation in the two arms will destructively interfere and no radiation will proceed down the guide (see Problem 9.15). It is easy to show that the output of the device will have a sinusoidal dependence on the applied field (see section 10.1.3.1 which deals with a very similar problem), and so if the device is biased at the half maximum transmission point the output irradiance will vary approximately linearly with applied field provided the field variations are small (see Fig. 3.10b for an illustration of this). Devices are commercially available, based mainly on lithium niobate, which have modulation capabilities of up to a few tens of gigahertz.

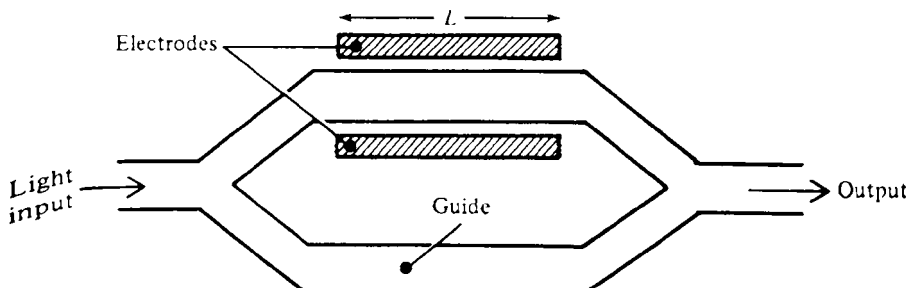


FIG. 9.38 Interferometric modulator; a voltage applied across the electrodes affects the refractive index of the upper guide over a distance L .

Some work has also been carried out into the possibility of using organic polymers in phase shift modulators. These materials offer the advantage of low cost and flexible processing techniques coupled with electro-optic coefficients which are as large, and possibly larger, than in lithium niobate. However, there are problems with high insertion losses (when used in conjunction with silica optical fibers) and the low thermal stability of the material. Semiconductor materials such as GaAs and InP do exhibit an electro-optic effect, but the electro-optic coefficients are not very large (see Table 3.1). However, semiconductor quantum well structures exhibit an electric-field-induced change in their effective refractive index which is much larger than in the bulk material.⁴ Although only some 10% of the mode field in such waveguides is actually within the quantum well structure, which reduces the effectiveness of the refractive index changes, the changes are still appreciably larger than in the bulk material. The interaction lengths required (i.e. the length L in Fig. 9.38) is thereby reduced from a few millimetres to several hundred micrometres. This has two main advantages: first it increases the device density on the substrate, thereby reducing costs; and secondly it reduces the electrical capacitance, thereby increasing the modulation bandwidth.

A different type of switch/modulator may be constructed which utilizes the coupling of energy between waveguides when they are brought into close proximity. We have met this phenomenon before when considering optical fiber couplers (section 8.5.2); it arises as a result of the overlap of the evanescent field in one guide with the core of the neighbouring guide. Using coupled mode theory it can be shown that (ref. 8.28) the amount of energy coupled into the neighbouring guide over a length z (Fig. 9.39) is proportional to the factor F_c , where, for identical waveguides,

$$F_c = \sin^2(Cz) \quad (9.27)$$

whilst for non-identical waveguides

$$F_c = \frac{C^2}{C^2 + \delta^2} \sin^2[z(C^2 + \delta^2)^{1/2}] \quad (9.27a)$$

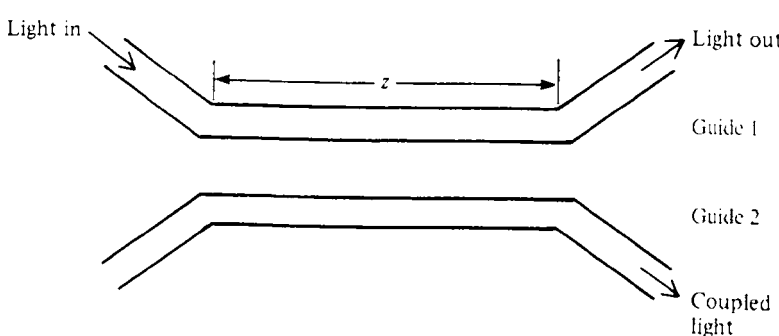


FIG. 9.39 Two waveguides in close proximity over a coupling distance z . As explained in the text evanescent field overlap can cause energy to be transferred between the guides.

Here, C characterizes the coupling between the guides and the factor δ is given by

$$\delta = \frac{\pi}{vc} (n_1 - n_{11})$$

where n_1 and n_{11} are the refractive indices of the two guide materials and v is the frequency of the radiation.

If $\delta = 0$, then after a coupling length $z = L_c$ where $L_c = \pi/(2C)$, all the power in one guide will be transferred to the other, whilst after a further distance L_c all the power will have been transferred back again (Fig. 9.40a). However, if $\delta \neq 0$ then not only is less energy exchanged but also the energy change takes place more rapidly with distance (Fig. 9.40b). Suppose that we have identical waveguides which can be changed to non-identical guides in some way. If the coupling length is equal to L_c then, whilst the guides are identical ($\delta = 0$), all the energy in one guide will couple into the other. However, if the guides are now made non-identical and with δ having a value such that $L_c(C^2 + \delta^2) = \pi$ (i.e. $\delta = \sqrt{3}C$), then over a coupling length L_c no energy is exchanged. This means we can switch energy from one waveguide to another provided we can 'switch' from a situation where $\delta = 0$ to one where $\delta = \sqrt{3}C$ (see Problem 9.16).

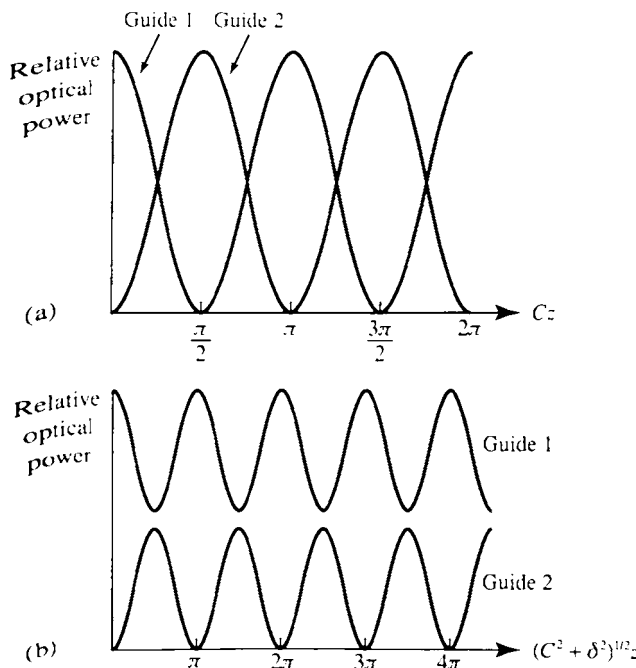


FIG. 9.40 Transfer of optical power between waveguides as a function of coupling distance z (see Fig. 9.39) according to eqs (9.27) and (9.27a). In (a) the guides are identical and all the energy is exchanged between the guides, whereas in (b) the guides are non-identical and only a partial exchange of energy is possible.

Several configurations have been built to implement this, of which the simplest is shown in Fig. 9.41. Electrodes are deposited above each waveguide and a potential is applied between them. The opposing vertical fields in the two waveguides can, if the material axes have been chosen correctly, induce opposite changes in the guide refractive indices and hence change the value of δ . The main problem with this arrangement is that it is not easy to achieve total energy transfer because of the difficulty of ensuring that the coupling length is exactly L_c . More complicated electrode configurations have been proposed to overcome these difficulties (ref. 9.18).

Devices such as filters and resonators may be realized in IO by incorporating periodic structures into optical waveguides. Consider, for example, a waveguide with a 'corrugation' etched upon its surface perpendicular to the direction of beam propagation (Fig. 9.42). This structure is encountered in the distributed feedback laser (section 6.2); it acts as a wavelength-dependent mirror, that is strong reflection occurs when $2D = m\lambda_0/n_1$, where D is the grating period, λ_0 the vacuum wavelength, n_1 the guide material refractive index and m an integer. Reflection bandwidths are usually narrow, but may be increased by 'chirping' the grating (Fig. 9.43).

Although all the devices discussed above use stripe waveguides, devices can also be based on slab waveguides. One of these is a beam deflector based on diffraction from an acoustic wave. An interdigital electrode structure deposited on a suitable acousto-optical material (see Fig. 9.44) can generate a beam of surface acoustic waves which can then serve to diffract light travelling along the guide. The angle through which the beam is diffracted may be changed by varying the frequency (and hence the wavelength) of the acoustic wave. This device is of course a version of the acousto-optic deflector discussed in Chapter 3.

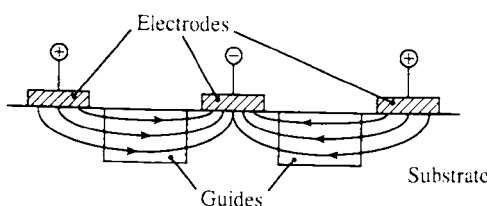


FIG. 9.41 An electrode configuration used to modify the propagation conditions in two adjacent waveguides in order to alter the coupling of radiation between them. The electric fields are in opposite directions through the guides and hence the effective refractive index of one guide will be raised whilst that of the other will be lowered.

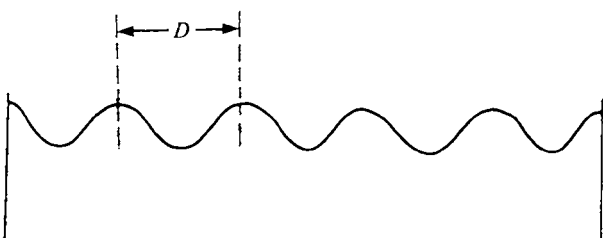


FIG. 9.42 Waveguide with a corrugation of period D etched upon it.

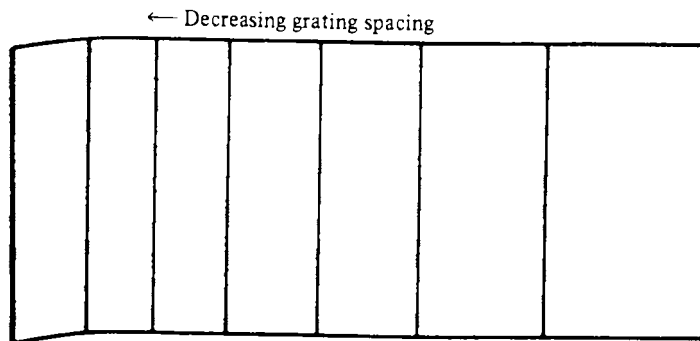


FIG. 9.43 'Chirped' diffraction grating structure. A plan view is shown with the vertical lines representing the grating peaks (or troughs).

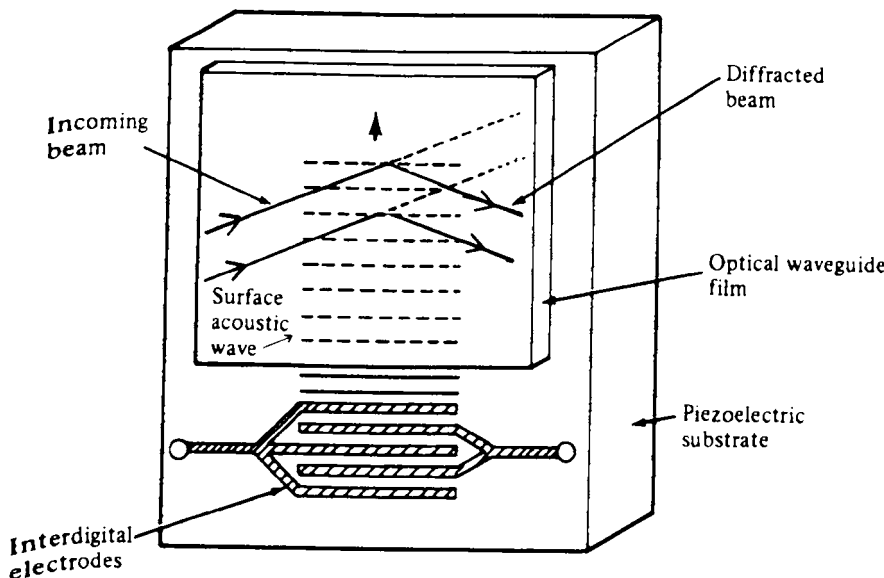


FIG. 9.44 Beam deflection using diffraction from a surface acoustic wave generated by applying an alternating voltage to an interdigital structure evaporated onto the surface of a piezoelectric substrate.

When it comes to emitters and detectors the most obvious choice for a substrate would seem to be a semiconductor. We have seen in Chapters 6 and 7 how efficient emitters and detectors can be made from them. However, many of the modulators/switches discussed above were based, not surprisingly, on materials such as lithium niobate, which exhibit relatively high electro-optic coefficients. Semiconductor materials such as GaAs and InP are electro-optically active but have appreciably smaller coefficients, as has already been pointed out. Thus the optimum substrate materials for modulators and emitters/detectors do not necessarily coincide. Since it is impossible for lithium-niobate-type materials to be made into emitters or detectors, it would appear that, if complete integration is required,

semiconductor substrates will have to be used, probably in conjunction with quantum well structure modulators which offer an increased electric field sensitivity.

In semiconductor lasers the radiation is generated within a channel of similar dimensions to those of stripe waveguides, which aids the coupling of power between them. Because of the difficulties of obtaining cleaved end mirrors, however, a distributed feedback structure (section 6.2) is usually employed, rather than the more common Fabry–Perot structure. One problem with the laser as a source is that, when not being pumped, the lasing region is absorbing; consequently arrangements are usually made for coupling the radiation from the active layer into a non-lossy guiding layer situated beneath it (see Fig. 9.45). Quantum well structures are attractive for lasers since they offer a number of advantages such as low threshold current, low temperature sensitivity and excellent dynamic behaviour as well as integrating well with modulators which are also based on quantum wells.

Finally in this section we deal with a class of devices known as ‘bistable optical devices’. In these devices two distinct optical states can exist with the possibility of switching between them. Such basic devices can form the basis of a whole series of logic gates (e.g. AND, NAND, OR and NOR gates). Furthermore if the elements can be switched by light itself then we have the basis of an all-optical computer (ref. 9.19). Such a switching device can be made by growing a multiple quantum well in place of the intrinsic region in a p-i-n photodiode (Fig. 9.46a). We suppose that light of irradiance I_{in} falls onto one face of the device and that an irradiance I_{out} emerges from the other side. The device is electrically biased using a battery and a load resistor R (and hence is known as an R-SEED). Because of the presence of the bias field the absorbance of the MQW structure is relatively small and thus for small values of I_{in} we will have that $I_{out} \approx I_{in}$. If I_{in} is now increased then so will the current flowing in the external bias circuit. As this current becomes larger so the bias actually applied to the device will fall and hence cause the absorption in the MQW region to increase (section 3.9). A point will be reached when the device suddenly switches to a state where the absorption in the MQW region is very high; a relatively large current flows in the bias circuit and the voltage across the cell is very small (which is what causes the absorption to be high). If now I_{in} is slowly reduced the high absorption state will persist for some time before the device equally suddenly switches back to the low absorption state as illustrated in Fig. 9.46(b); thus the switching process exhibits hysteresis. Suppose we

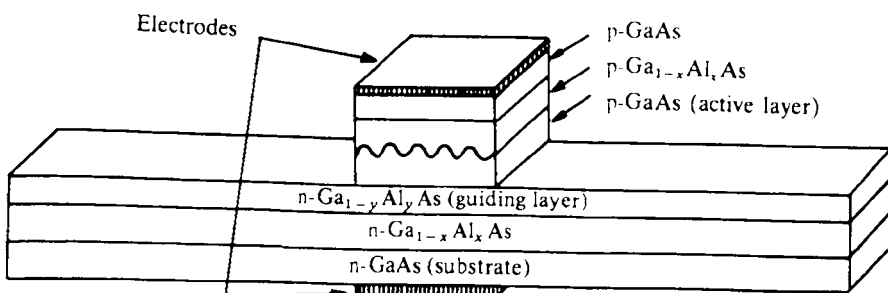


FIG. 9.45 IO semiconductor laser based on GaAs/GaAlAs using Bragg reflectors instead of cleaved end mirrors. Light from the active layer is coupled into the layer beneath, which then acts as a waveguide.

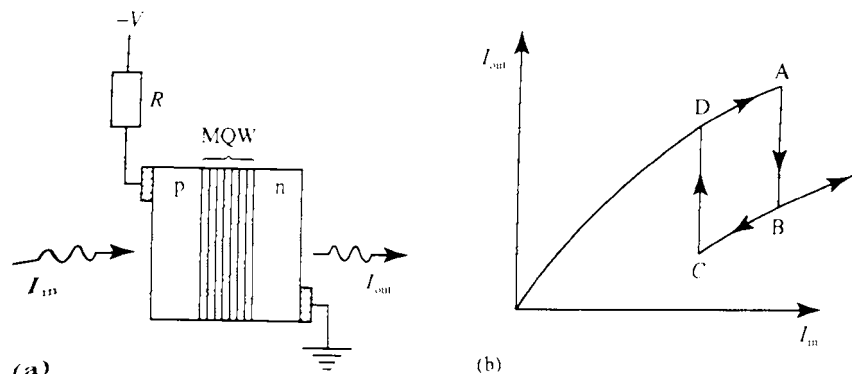


FIG. 9.46 (a) The basic structure of an R-SEED switching device. (b) The relationship between the incident (I_{in}) and transmitted (I_{out}) irradiances. As explained in the text the device exhibits a hysteresis loop.

have a bias beam of irradiance I_b where I_b is such as to be just less than the irradiance at which the device switches from low to high transmission states and that, in addition, we have a signal beam I_s where the combined irradiance $I_b + I_s$ is such as to cause the device to switch just to the low transmission state. If the device is then permanently illuminated with the bias beam, the presence or absence of the signal beam will cause the device to switch between low and high transmission states. Unfortunately it is not usually practicable to maintain the constancy of the bias beam with the required accuracy. This problem can be solved by replacing the bias resistor with another SEED device, thus generating the symmetric SEED or S-SEED (Fig. 9.47). The most important feature of the S-SEED is that changes of state occur if the ratio of the two input power irradiances alters; changes in the

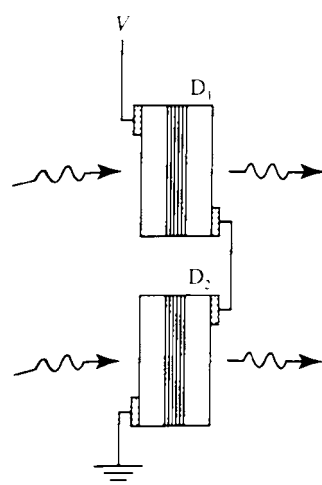


FIG. 9.47 Two SEED devices (D_1 and D_2) connected together to form an S-SEED.

absolute irradiances of the input beams do not cause a change of state. The output of the device consists of a pair of light beams, one of which will be in the 'on' or high irradiance state, the other in the 'off' or low irradiance state. In *single rail logic* the signal beam is only incident on one of the devices, but other pulses must be applied to both elements. Suppose, for example, that a logical AND operation is required, the sequence of operation is as follows:

1. Initial 'preset' pulses are applied so that device 1 is set at high ($D_1 = 1$) and device 2 at low ($D_2 = 0$).
2. The input signal pulses, S_a and S_b , are applied to device 1.
3. 'Clock' pulses are applied to both devices: the result of a logical AND operation may then be read from the output of device 2 and of a logical NAND from the output of device 1.

Suppose, for example, that $S_a = 0$ and $S_b = 1$; after S_a there will be no change in the state of the detectors, but after S_b the detectors' states will switch, so that $D_1 = 0$ and $D_2 = 1$. The clock pulse will then read a logical 1 from device 2 as required (and a logical 0 will be read from device 1, giving a NAND operation). The logical operations OR and NOR can similarly be obtained by initially setting $D_1 = 0$ and $D_2 = 1$. By combining S-SEED devices more complex devices can be constructed, for example a 2×2 switching element can be constructed by using six S-SEED elements (ref. 9.20).

9.4.3 IO devices

One of the earliest IO devices to be fabricated was an optical spectrum analyzer, designed to display the frequency spectrum of a radio-frequency (RF) signal (ref. 9.21). The layout is illustrated in Fig. 9.48. Light from a semiconductor laser is launched into a waveguide and the beam subsequently rendered parallel by the use of a 'geodesic' lens. This is a circular indentation made in the substrate layer with the guide layer thickness being unchanged across the indentation (Fig. 9.49). Such a structure behaves like a 'one-dimensional' lens (ref. 9.22). The parallel beam then passes through the acousto-optic beam deflector. If a single RF frequency is present, the amount of deflection will depend on the instantaneous value of the frequency. A second lens subsequently focuses the light onto a particular photodetector in a photodetector array. Each detector element corresponds to a particular frequency (or, more accurately, a narrow range of frequencies). If, in fact, more than one frequency is present, the light will be divided into different components that are then focused onto different elements, thus enabling the frequency spectrum of the RF signal to be obtained. The device as illustrated here is obviously a 'hybrid' since the emitters and detector elements are separate devices which are merely attached to the edge of the substrate.

Some more recent integrated devices have involved the integration of electronic components (usually gain devices based on transistors) with optical elements. For example, a Pockels-effect-type modulator can be driven from the input of a transistor amplifier so that the actual electrical input signal to the device can be relatively small. Other candidates are the drive circuits for laser emitters and the front end amplifier for an optical detector. As an example of the latter, Fig. 9.50 shows a (simplified) schematic diagram of an MSM photodiode (section

Chapter 20

Applications of Integrated Optics and Current Trends

In the preceding chapters, the theory and technology of optical integrated circuits have been described. Although this a relatively new field of endeavor, numerous applications of OIC's to the solution of current engineering problems have already been implemented and some OIC's are now available as "off-the-shelf" commercial products. Of course, optical fiber waveguides, the companion element of OIC's in an integrated-optic system, are already well recognized as being very useful consumer products. In this chapter, some of the more recent applications of both fibers and OIC's are reviewed, and current trends are evaluated. In this review of representative integrated optic applications, specific systems and companies are named in order to illustrate the international character of the field and the types of organizations that are involved in it. Recommendation of any particular company or its products is not intended or implied. Also, the performance data that are quoted have generally been obtained from news articles and other secondary sources. Hence, they should be interpreted as being illustrative rather than definite.

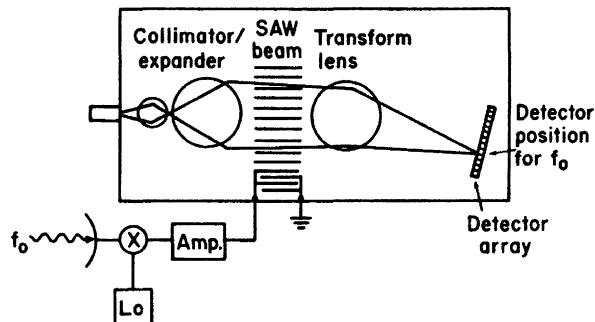
20.1 Applications of Optical Integrated Circuits

20.1.1 RF Spectrum Analyzer

Probably the earliest demonstration of a multi-element OIC that was performed was the hybrid implementation of the real-time rf spectrum analyzer, which was originally proposed by Hamilton et al. [1]. The purpose of this spectrum analyzer, is to enable the pilot of a military aircraft to obtain an instantaneous spectral analysis of an incoming radar beam, in order to determine if his plane is being tracked by a ground station, air-to-air missile, etc. Obviously, such information is required if he is to be able to quickly take effective evasive action. Of course, the frequency content, or *signature*, of all enemy radar signals that are likely to be encountered would have to be available for comparison, probably stored in the memory of the plane's onboard computer.

A diagram of the integrated-optic spectrum analyzer is shown in Fig. 20.1. Light from a laser source is coupled into a planar waveguide, in which it passes first

Fig. 20.1 Diagram of an integrated-optic rf spectrum analyzer



through a collimating lens, then through a Bragg-type acousto-optic modulator. The rf signal to be spectrally analyzed is applied to the acoustic transducer that generates the sound waves, causing them to have a time varying period. Thus the deflection angle of the optical beam at the output of the modulator is a function of the rf signal. A second lens is used to focus the optical beam onto an array of photodetectors. If more than one frequency component is present in the rf signal, the light beam is divided into corresponding components that are focused onto different detector elements. Each detector element represents a particular frequency channel, and, since photo-diodes generally have square law response, the output signal from any channel is proportional to the rf power at that frequency. The advantage of an integrated-optic spectrum analyzer, as compared to an electronic one, is that only a few optical elements are needed to perform a function that would otherwise require thousands of electronic elements.

The development of working models of the integrated optic rf spectrum analyzer took place at several different laboratories and extended over a number of years. The first working model was produced by the Westinghouse Advanced Technology Laboratories in 1980 [2, 3]. It was fabricated on an X-cut LiNbO₃ substrate, approximately $7 \times 2.5 \times 0.3$ cm³, in which a planar waveguide had been produced by indiffusion of titanium at 1000°C. The lenses used were of the geodesic variety, formed by machining *dimples* into the surface of the substrate prior to waveguide diffusion. In this type of lens, light waves are still confined by the waveguide, but they follow the longer curved path through the lens region. Since waves traveling near the center of the lens go over a greater path length than waves traveling near its edges, the wavefront is modified, so that focusing can occur. Such lenses can be made with surprising accuracy. The two aspherically-corrected geodesic lenses in the Westinghouse spectrum analyzer had essentially diffraction-limited spot sizes. The silicon diode detector array contained 140 elements, and was butt coupled to the waveguide. Design parameters for the Westinghouse integrated-optic spectrum analyzer are shown in Table 20.1. The input lens focal length was chosen to expand a 6 μm GaAlAs laser spot to 2 mm by diffraction.

The spectrum analyzer was tested first with a He-Ne laser source of 6328 Å wavelength and found to have a bandwidth of 400 MHz with a resolution of 5.3 MHz.

Table 20.1 Westinghouse spectrum analyzer, design parameters [2, 3]

Substrate size	$7.0 \times 2.5 \text{ cm}^2$
Front face to collimating lens	2.45 cm
Collimating lens diameter	0.80 cm
Collimating lens focal length	2.45 cm
Spacing between lenses	1.80 cm
Transform lens offset angle	3.79°
Transform lens offset	0.06 cm
Transform lens focal length	2.72 cm
Detector array pitch	12 μm
Laser beam width	6 μm
Number of detector elements	140
SAW transducer type	2 element, tilted

Later results obtained by using a butt-coupled GaA1As laser diode emitting at 8300 Å as the source showed an improved resolution of 4 MHz. Other performance characteristics are given in Table 20.2. The 400 MHz bandwidth limitation is mostly caused by the acoustic transducer, and may be improved by using a more sophisticated transducer, as described in Chapter 10. In any case, the spectrum analyzer could be used over a wider frequency range by using a local oscillator and mixer at the input to the transducer, as shown in Fig. 20.1. Thus, heterodyning could be used to electronically shift the 400 MHz bandpass to various center frequencies as desired.

Shortly after a working model of an rf spectrum analyzer was demonstrated by Westinghouse, an alternate embodiment of essentially the same design was demonstrated by Hughes Aircraft Company. The Hughes OIC also followed the basic pattern proposed by Hamilton et al. [1], as shown in Fig. 20.1. However, it differed from the initial Westinghouse OIC in that it featured a butt-coupled GaA1As laser diode rather than a He-Ne laser source, and the detector array was composed of silicon charge-coupled-devices (CCD) [4, 5] rather than photodiodes. The Hughes spectrum

Table 20.2 Westinghouse spectrum analyzer, performance characteristics [2, 3]

Center frequency	600 MHz
Frequency bandwidth	400 MHz
Frequency resolution	
with He-Ne 6328Å source	5.3 MHz
with GaA1As 8300Å source	4 MHz
Detector integration time	2 μs
Detector element spacing	12 μm (with no dead space between elements)
Full width at half power of focused spot in detector focal plane	3.4 μm ($1.02 \times$ diffraction limited size)
Bragg diffraction efficiency	50 to 100%/w

analyzer exhibited a 3 dB bandwidth of 380 MHz with a diffraction efficiency of 5% (at 500 mW rf power) [6, 7]. Operating at a wavelength of 8200 Å, the OIC had a resolution of 8 MHz and a linear dynamic range greater than 25 dB. Losses in the two geodesic lenses were measured to be less than 2 dB each.

The two embodiments of the rf spectrum analyzer described above are excellent examples of hybrid optical integrated circuit technology. By fabricating the laser diode in GaAlAs, the detector array in silicon, and the Bragg modulator in LiNbO₃, one can use the best features of all three materials to advantage. The major disadvantage of the hybrid approach is that all of these substrate materials must be carefully aligned and permanently bonded with micrometer-tolerance precision. Thermal expansion and vibration must somehow be prevented from destroying the alignment. Despite these difficulties, hybrid OIC's have been demonstrated to be viable structures, and will continue to be used in many applications even after monolithic technology has been fully developed.

20.1.2 Monolithic Wavelength-Multiplexed Optical Source

One of the applications for which optical integrated circuits were proposed early in the history of the field is an optical-frequency-multiplexed transmitter, such as that shown previously in Fig. 1.1, in which a number of DFB lasers, operating at different wavelengths, are coupled into a single fiber transmission line. An OIC of this type has, in fact, been fabricated by Alki et al. [8], using GaAlAs monolithic technology. Six DFB lasers, operating at wavelengths separated by 20 Å, were fabricated on a 5 mm square GaAs substrate by a two-step LPE growth process. The lasers had a separate confinement heterostructure (SCH) [9]. Third-order gratings were made on the surface by chemical etching, by using a mask made by holographic lithography. The lasers were coupled to undoped Ga_{0.9}Al_{0.1}As waveguides by direct transmission, as shown in Fig. 20.2. The lateral dimensions of the lasers and waveguides were defined by mesa etching down to the GaAs substrate to produce stripes that were 20 μm wide and 3 μm thick. The separation of the lasers was 300 μm, and the waveguides were curved through bends of minimum radius equal to 4 mm, in order to bring them together in a confluent coupler, as shown in Fig. 20.3. The output of the coupler was obtained via a single waveguide that was butt coupled to an optical fiber.

The lasers were operated by applying 100 ns current pulses at a repetition rate of 1 kHz. The differential quantum efficiency of the lasers was measured to be 7%, and the waveguide loss coefficient was about 5 cm⁻¹. The threshold current densities of the lasers were in the range from 3 to 6 kA/cm² at room temperature. The wavelength separation between lasers was measured to be 20 ± 5 Å. No difficulty was encountered in separately modulating the six lasers, and the overall differential quantum efficiency, measured at the launching output terminal, was about 30%. Thus, this early version of a monolithic chip represented a usable OIC, even though further refinements were to yield better efficiency.

Work on monolithic wavelength-multiplexed optical sources employing DFB lasers has continued over the years, with more recent work being directed toward

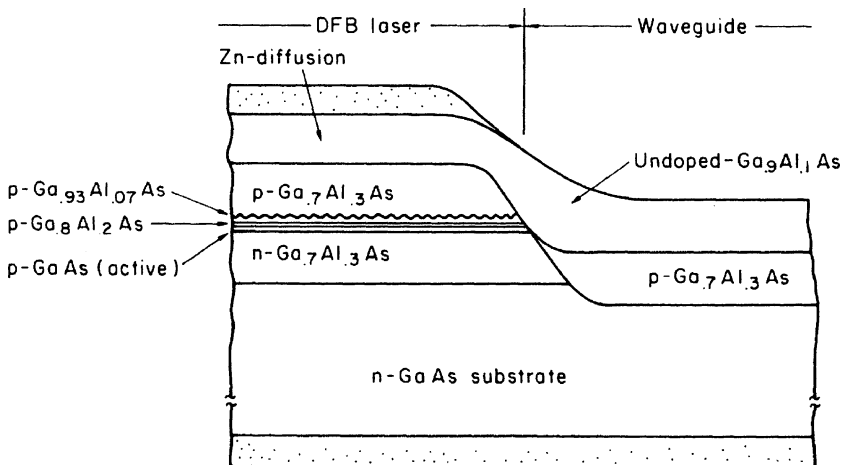


Fig. 20.2 DFB laser coupled to a GaAlAs waveguide by direct transmission [9]

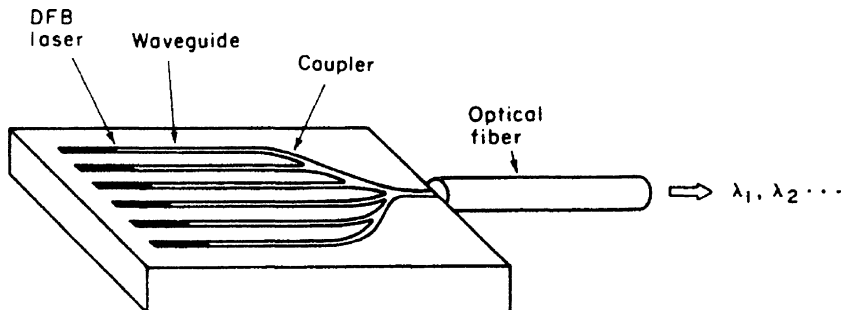


Fig. 20.3 Schematic drawing of a wavelength-multiplexed light source [8]

1.3 μm and 1.55 μm wavelength lasers for optical-fiber telecommunication systems. Zah et al. [10] have reported a study of wavelength-division multiplexed lighwave systems which has led to the conclusion that, in order to be cost effective, it is necessary to fabricate multi-wavelength laser transmitters by monolithic integration on one chip to reduce the cost of packaging and control circuitry by sharing them among all of the wavelengths. An example of such monolithic integration is provided by the frequency-division multiplexed ten-channel tunable DFB laser array of Sato et al. [11]. The lasers are tunable, multi-section, quarter-wave-shifted, strained InGaAsP MQW devices. The lasing frequencies of channels are spaced within a 10 GHz range. The linewidth of each channel is less than 2.3 MHz. A monolithically integrated chip containing 21 DBR lasers has been produced by Lee et al. [12]. They used sampled grating distributed Bragg Reflectors, in which the grating is not continuous, but rather is formed in bursts so that it has two inherent periodicities. This type of DBR grating makes the selection of laser emission wavelength more

accurate. The 21 InP/InGaAsP MQW lasers on the chip had emission wavelengths spanning over 40 nm with 0.8 nm spacing, centered at approximately 1.56 μm .

20.1.3 Analog-to-Digital Converter (ADC)

An analog-to-digital conversion method, proposed by Taylor [13, 14], has been implemented by Yamada et al. [15] in an optical integrated circuit that is capable of one-bit electro-optical AD conversion at a 100 MHz rate. The OIC incorporates two 3-dB couplers and a phase shifter, formed in a pair of straight waveguides, as shown in Fig. 20.4. The waveguides were fabricated by Ti diffusion of a LiNbO_3 substrate. The phase shifter was formed by a Ti double-diffusion, as shown in Fig. 20.4. An Al_2O_3 1100 Å thick buffer layer was used, separated by a 4 μm , gap between the waveguides to suppress dc drift. Waveguide spacing was 5.4 μm and device length was about 2 cm.

The configuration of two electro-optic couplers and a phase shifter forms a balanced-bridge modulator, with two complementary outputs which are equally affected by fluctuation of the light source. Hence a serious source of conversion error is inherently eliminated in this OIC. The integrated ADC was operated with a 1.15 μm -wavelength He-Ne laser source at bit rates up to 100 MHz. This initial success of high speed analog-to-digital conversion points the way towards more sophisticated, multi-bit, and monolithic OIC's. However, much remains to be done, especially in regard to development of a monolithic, high-speed, electronic or optical comparator to be incorporated into a fully monolithic ADC system.

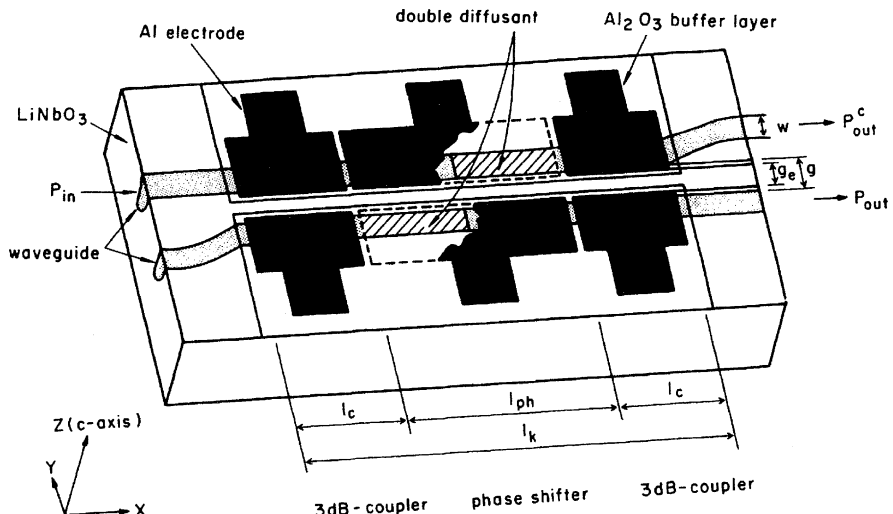


Fig. 20.4 Diagram of an integrated-optic analog to digital converter [15]

As work continues on these devices, optoelectronic ADCs capable of multibit conversion have been developed [16–21]. A twelve bit ADC developed by Twichell and Helkey [21] relies on a gain-switched diode laser and a dual-output Mach-Zehnder interferometer to produce phase-encoded sampling. Currie et al. [19] have produced a photonic ADC that maps an analog input waveform into a binary output by employing phase modulators and polarization-based optics.

20.1.4 Integrated-Optic Doppler Velocimeter

An integrated-optic Doppler velocimeter which employs both an optical fiber link and an OIC to measure velocity has been demonstrated by Toda et al. [22], as shown in Fig. 20.5. The optical integrated circuit was fabricated in a z-propagation LiNbO_3 substrate with Ti diffused waveguides. Laser beam lithography, with $0.2 \mu\text{m}$ accuracy, was used for waveguide patterning. The light source was a linearly polarized He-Ne laser. TE polarized light was focused into the input waveguide by a 20% lens and then split by a Y-branch coupler into a signal beam and a reference beam. TE polarization was maintained on outgoing light while TM polarization was used for reflected light. Of course, polarization-maintaining optical fiber was used. In the case of the reference beam the TE/TM conversion was accomplished by means of an electro-optic mode converter. For the signal beam a quarterwave plate was used to produce TE/TM mode conversion. An absorptive TE/TM mode splitter was used to route the return signal beam to the avalanche photodiode (APD) which served as

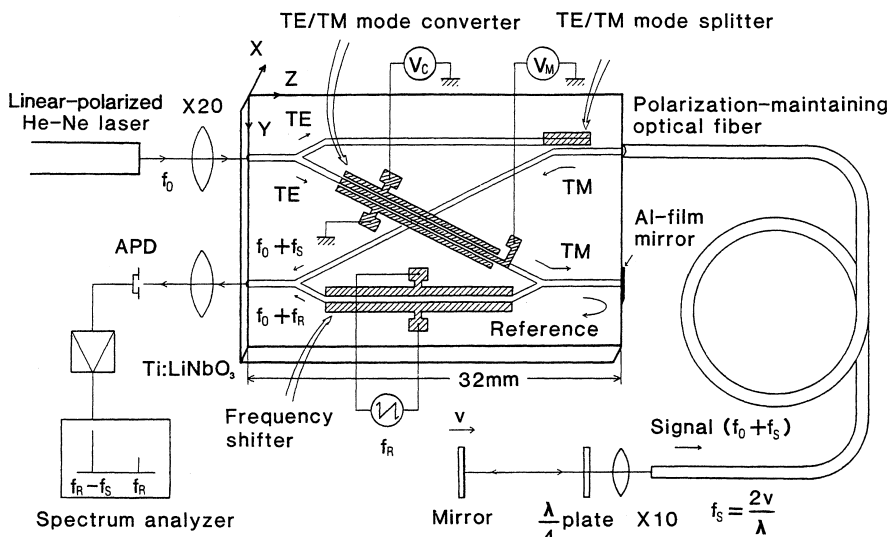


Fig. 20.5 An integrated-optic Doppler velocimeter

a mixer and detector. An electro-optic modulator was used to impress the reference modulation frequency f_R onto the reference beam. The Doppler effect produced a shift in the signal beam frequency from f_0 to $f_0 + f_s$, where f_s is given by

$$f_s = \frac{2v}{\lambda_0}, \quad (20.1)$$

where v is the velocity and λ_0 is the vacuum wavelength. After being recombined by a Y-branch coupler the reflected signal beam and reference beam were mixed in the avalanche diode. Because of the nonlinear response characteristic of the APD (it is a square-law device, i.e., response is proportional to the square of the electric field strength) the output photocurrent contained a beat frequency component $f_R - f_s$. Thus f_s , and hence the velocity, was determined. For a velocity of 8 mm/s the measured f_s was 25 kHz, and the signal to noise ratio was 25 dB.

This Doppler velocimeter demonstrates that integrated-optic technology can provide the compact and rugged heterodyne optics need for highly accurate measurement of velocity and displacement. By adding a balanced-bridge waveguide optical switch to an interferometric circuit of this type Toda et al. [23] have produced a time-division-multiplexed Doppler velocimeter which can measure two-dimensional velocity components v_x and v_y .

20.1.5 An IO Optical Disk Readhead

Optical disk information storage has found widespread use for computer data, as well as for video and audio reproductions. High data density and low background noise are key advantages of this method. However, relatively sophisticated optics must be used to insure good resolution and tracking of the light beam that is used to read information off the disk. For example, the optical readheads used in commercially available audio compact disk (CD) players often have eight or nine discrete optical elements, all of which have to be held in exact alignment in the face of much shock and vibration.

As an alternative, an integrated-optic optical disk pickup device capable of detecting readout and focus/tracking error signals has been designed and fabricated by Ura et al. [24], as shown in Fig. 20.6. The OIC was formed by depositing a planar # 7059 glass waveguide on a SiO_2 buffer layer on a silicon substrate. The light source was a butt-coupled GaAlAs laser diode. A chirped and curved focusing grating pattern coupler fabricated by electron beam direct writing lithography was used to focus the beam onto the disk, as well as to refocus the reflected beam back into the waveguide. A twin-grating focusing beam splitter served to divide the reflected beam into two beams which were focused onto two pairs of photodiodes formed in the Si substrate.

In operation, the pickup head provides not only a readout signal but also focus and tracking error signals. When the light beam is focused, the return beams hit both diodes of each pair equally. If the readhead is too close to the disk, the beams

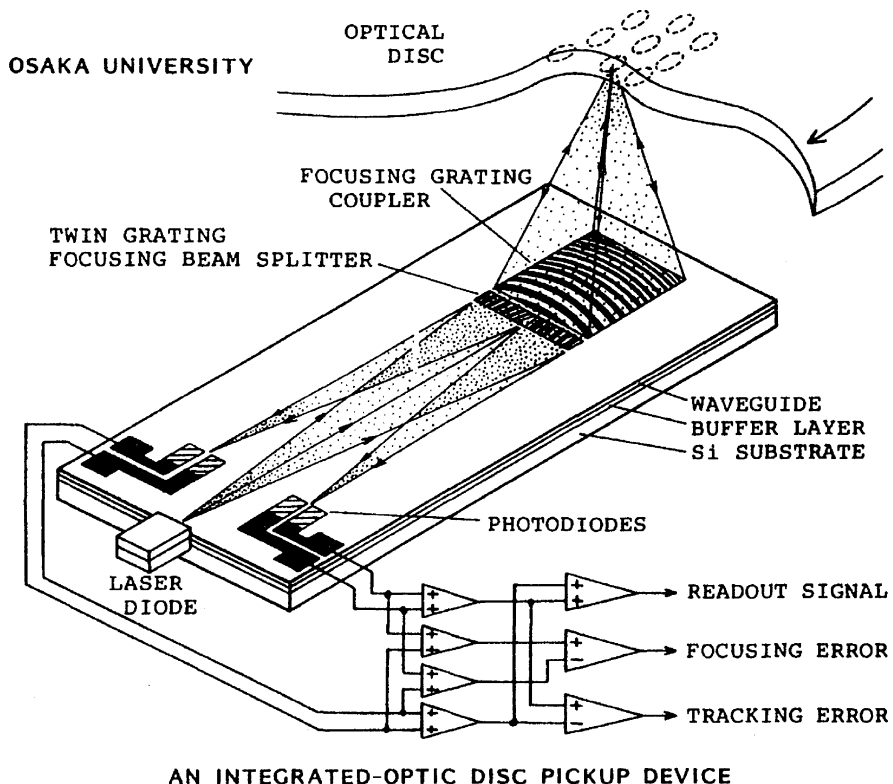


Fig. 20.6 An integrated-optic disc pickup device [24]

fall more on the outer diodes, while if it is too far away they fall more on the inner diodes. Tracking error is detected when the total intensity of the return beam reaching the left pair of diodes is not equal to that reaching the right pair. Thus conventional electronic comparators, sensing the photo-currents from the diodes, can be used to develop error signals to drive position correcting actuators.

The OIC readhead of Fig. 20.6, which has dimensions of only 5×12 mm, obviously has the advantage of being relatively insensitive to shock and vibration, as compared to a readhead fabricated from discrete optical components. While this OIC was first proposed as an optical disk pickup device, the same basic arrangement can be used more generally as a fully integrated interferometer position/displacement sensor with direction discrimination [25]. Such an interferometric sensor would be useful in a variety of high-precision positioning applications in which submicrometer accuracy is required.

An integrated optical disk readout head has also been made by Hudgings et al. [26]. Their device makes use of a vertical cavity surface emitting laser with an intra-cavity quantum well absorber. Detection of the reflected optical signal is performed by measuring the change in absorber voltage as the optical feedback into the VCSEL

cavity varies. The head has a $0.22 V_{pp}$ response Its RC time constant is $20 \mu s$, indicating a 50 kHz rolloff frequency.

Manoh et al. [27] have reported an integrated optical head device using a blue-violet laser diode. This head, which integrates seven optical elements and semiconductor chips into a $11 \text{ mm} \times 6 \text{ mm} \times 4.1 \text{ mm}$ package, is a key device for realizing a small and thin Blu-ray Disc drive.

20.1.6 OIC Temperature Sensor

The integrated-optic temperature sensor [28] shown in Fig. 20.7, requires no electrical connection, making it particularly useful in explosive or flammable environments in which an electrical sensor might be dangerous. The OIC is fabricated in a LiNbO_3 substrate with Ti diffused waveguides. It features a parallel array of three unequal arm-length Mach-Zehnder interferometers. The optical transmission of each interferometer varies sinusoidally with temperature, as shown in Fig. 20.7b, with a period which is inversely proportional to the optical path length difference between the two arms.

The optical transmission $P_{\text{out}}/P_{\text{in}}$ at the wavelength λ depends on both the effective index n_{eff} and the path length difference ΔL and is given by [28]

$$\frac{P_{\text{out}}}{P_{\text{in}}} = \frac{\gamma}{z} \left[1 + m \cos \left(\frac{2\pi}{\lambda} b \Delta L T + \Delta\phi_0 \right) \right], \quad (20.2)$$

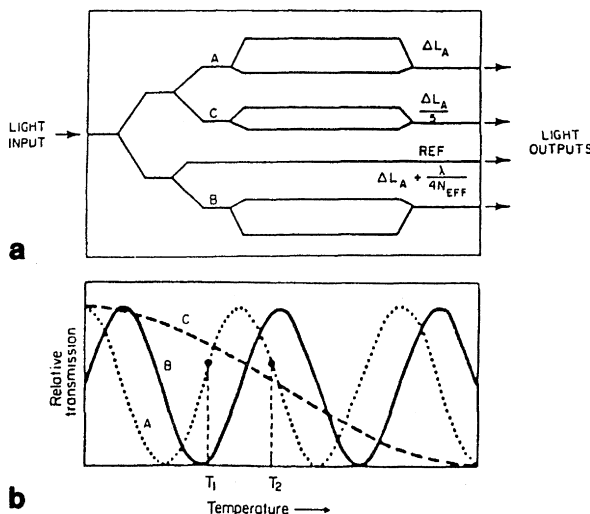


Fig. 20.7 a,b OIC temperature sensor **a** device structure **b** optical transmission characteristics [28]

where the constant of proportionality b is given by

$$b = \frac{dn_{\text{eff}}}{dT} + \frac{n_{\text{eff}}}{\Delta L} \frac{d(\Delta L)}{dT}. \quad (20.3)$$

Both n_{eff} and ΔL are functions of temperature T . The quantities γ and m are related to the insertion loss and depth of modulation of the interferometer, respectively. (For an ideal device $\gamma = m = 1.0$.) $\Delta\phi_0$ is a constant for a given device.

By measuring the transmission of all three interferometers one can determine the temperature. Two of the interferometers (A and B) have arm-length differences that are almost the same. Thus their transmission curves track close to one another, providing a high resolution in the temperature measurement. The third interferometer (C) has an arm-length difference which is only approximately one-fifth those of A and B. Thus one can determine which peak of the A and B transmission curves is being measured and temperature measurements can be made over a wide range. It has been reported that this temperature sensing OIC can measure with an accuracy of $2 \times 10^{-3}^\circ\text{C}$ over a 700°C range, when used with a 6328 \AA He-Ne laser as the light source. The sensor, of course, would be mounted at the point at which temperature measurement was desired and the optical input and output would be via optical fiber. Since the OIC chip is about 1 cm on a side, temperature measurements can be made on relatively small objects. Since the measurement signal is entirely optical, this device is relatively immune to electrical noise.

20.1.7 IO High Voltage Sensor

Integrated-optic Mach-Zehnder interferometers can be used to sense high voltage as well as temperature. A diagram of such a device is shown in Fig. 20.8 [29]. The waveguides are formed by Ti diffusion into a LiNbO_3 substrate. In this circuit the

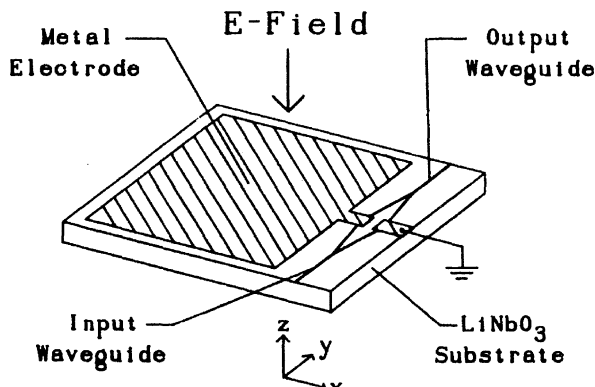


Fig. 20.8 IO high voltage sensor [29]

two branches of the interferometer are covered by metal electrodes which form a capacitive voltage divider. The electric field generated by the high voltage source induces a voltage on these electrodes which causes a relative phase shift between the optical waves in each arm, resulting in an intensity modulation of the output beam. The voltage-in/optical power-out transfer function is given by [29]

$$P_{\text{out}} = \frac{\alpha P_{\text{in}}}{2} \left[1 + \gamma \cos \left(\frac{\pi V}{V_\pi} + \phi_i \right) \right], \quad (20.4)$$

where P_{in} is the input power, ϕ_i is the intrinsic or zero voltage phase difference. V is the applied voltage and V_π is the half-wave phase shift voltage. The constants α and γ must be determined for a particular device. (For a perfect device $\alpha = \gamma = 1.0$.) Once the calibration curve has been determined for a particular sensor, the voltage can be accurately measured.

Since this sensor operates on the principle of an induced voltage it is not necessary to make electrical contact to the high voltage source, and input to, and output from the sensor can be via optical fiber. Thus good high voltage isolation can be maintained. The immunity to electrical noise provided by an optical fiber link is also a particularly important advantage when operating in a high voltage environment. This integrated optical high voltage sensor could be used, for example, for monitoring line voltages in SF₆-gas insulated bus ducts such as are used in power plants and switching stations.

20.1.8 IO Wavelength Meters and Spectrum Analyzers

By carefully arranging wavelength-selective optical elements in an OIC it is possible to make instruments that can measure an emission wavelength or spectrum. For example, Nabiev et al. [30] made a spectrophotometer that consists of two p-n junction InGaAs/GaAs QW photodiodes stacked vertically with a DBR reflector between them, as shown in Fig. 20.9a. The DBR reflector is composed of 10½ pairs of AlAs/GaAs. Lightwaves entering the top surface pass through both photodiodes and are detected by them. However, because of the wavelength selective reflectance of the DBR, some of the incident light doesn't reach the bottom photodiode. The ratio of the top detector response to that of the bottom diode is given by:

$$\frac{I_{\text{top}}}{I_{\text{bot}}} = R_0 \frac{1 + R(\lambda)}{1 - R(\lambda)}, \quad (20.5)$$

where R_0 is a constant of proportionality. The ratio of (20.5) is a single-valued function of wavelength that can be used to measure it, as shown in Fig. 20.9b, where the dotted curves are I_{top} and the solid curves are I_{bot} . The curve in (c) is a superposition of measurements at the three optical power levels shown in (b), indicating that measured wavelength is not sensitive to optical power.

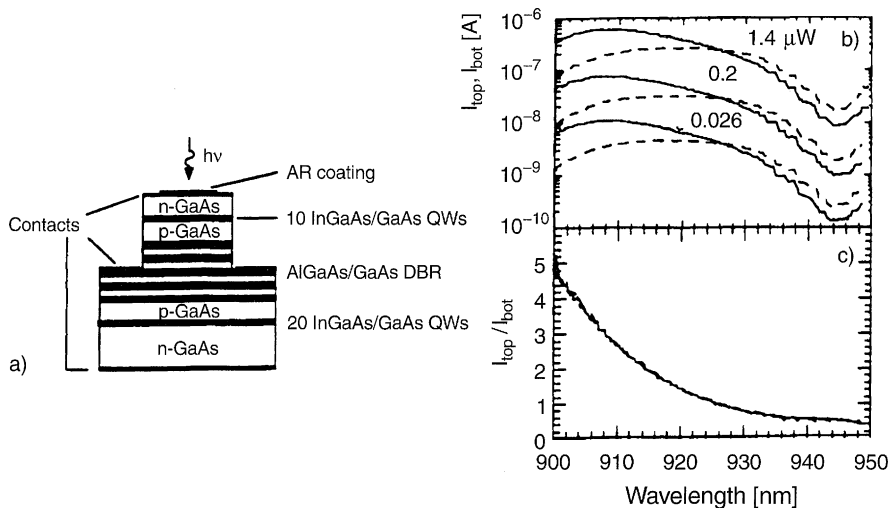


Fig. 20.9 a,b,c. Wavelength meter **a** device structure **b** response curves **c** response ratio [30] © 1995 IEEE

An integrated optic device also can be used to measure an optical spectrum as well as just a single wavelength. For example, an OIC optical spectrum analyzer has been described by Madsen et al. [31]. Their device uses a tilted, chirped grating in a planar single-mode waveguide to diffract lightwaves of different wavelengths through different angles as they are coupled out of the waveguide. The light radiated out of the waveguide is captured by a vertical slab waveguide that directs it to a linear array of photodetectors. Each detector intercepts light of only a narrow range of wavelengths, so the optical spectrum of the light can be determined. The full-width half-maximum resolution was 0.15 nm over a bandwidth range of 7.8 nm. In this device the grating, which has a chirp of -1.75 nm/cm and a focal length of 12 cm, performs both the spatial dispersion and imaging (focusing) functions.

20.1.9 IO Chemical Sensors

Integrated optic devices can be used to sense the presence and the concentration of various chemical elements. These sensors generally function by measuring the change in some optical property of the material in a waveguide that is produced by the presence of the chemical to be sensed. Both absorption spectro-photometry and attenuated total reflection spectrometry can be used, as well as fluorescence spectrometry. The waveguide may be either an optical fiber or a multilayer guide in an OIC. An example of this type of sensor is the thin-film polyvinyl chloride (PVC) co-polymer sensor reported by Kim et al. [32]. When doped with (HDOPP-Ca), a neutral ionophore for calcium, dioctyl phthalate (DOP), and the chromoionophore (ETH5294) the PVC waveguide showed enough chemical reaction to the Ca^{2+} ion

to measure its concentration when the waveguide was brought in contact with a solution of CaCl_2 . The absorption characteristics of the doped PVC waveguide in the range from 500 to 700 nm are changed by the presence of Ca^{2+} , causing a reduction in absorption and a shift of the peak to shorter wavelength. These changes can be calibrated with respect to calcium concentration. The use of different dopants can be expected to make the waveguide sensitive to the ions of other elements.

20.2 Opto-Electronic Integrated Circuits

In the optical integrated circuits described in Section 20.1 all of the key elements were optical devices. However, there is another class of optical integrated circuits in which many of the devices are purely electronic and the signal is carried in parts of the circuit by electrical voltage or current waves rather than by an optical beam. Such circuits have come to be called opto-electronic integrated circuits (OEIC's). They are usually fabricated on substrates of semi-insulating GaAs or InP because both electronic and optical devices can be monolithically integrated on these materials. However, a silicon substrate also can be used when a hybrid approach is used, with light emitters being made in a III-V material.

20.2.1 An OEIC Transmitter

An OEIC four-channel optical transmitter is shown in Fig. 20.10 [33]. This circuit was fabricated on a semi-insulating GaAs substrate by molecular beam epitaxy. It features an array of four stripe-geometry, single-quantum-well GaAlAs lasers with microcleaved facets. Each laser is accompanied by a photodiode to monitor output power and a driver circuit containing three field effect transistors (FET's). The lasers have a relatively low threshold current of 15–29 mA and a differential quantum efficiency of 50–60%. The emission wavelength is 834 nm. The FET's are Schottky-barrier-gate devices. By monolithically integrating electronic and optical devices in an OEIC such as this, one can reduce parasitic capacitance and inductance to a minimum, thereby increasing the achievable maximum frequency of operation. In the circuit shown in Fig. 20.10 the transmitter is capable of operating at a data rate of 1.5 Gb/s. Matsueda and Nakamura [34] have produced a single-channel OEIC transmitter featuring a four FET driver circuit, a monitor photodiode and a GaAlAs laser diode, all monolithically integrated on a GaAs semiinsulating substrate. That OEIC is capable of operating at a data rate of 2 Gb/s. Other OEIC transmitters are described in a review paper by Matsueda [35].

A four-channel laser transmitter OEIC for operation at $1.55 \mu\text{m}$ wavelength has been produced by Woolnough et al. [36]. It incorporates on an InP substrate, four single-mode, ridge-waveguide, InGaAsP, DFB lasers operating in the 1545 to 1560 nm window with 0.8 nm separation between adjacent channels. The drive

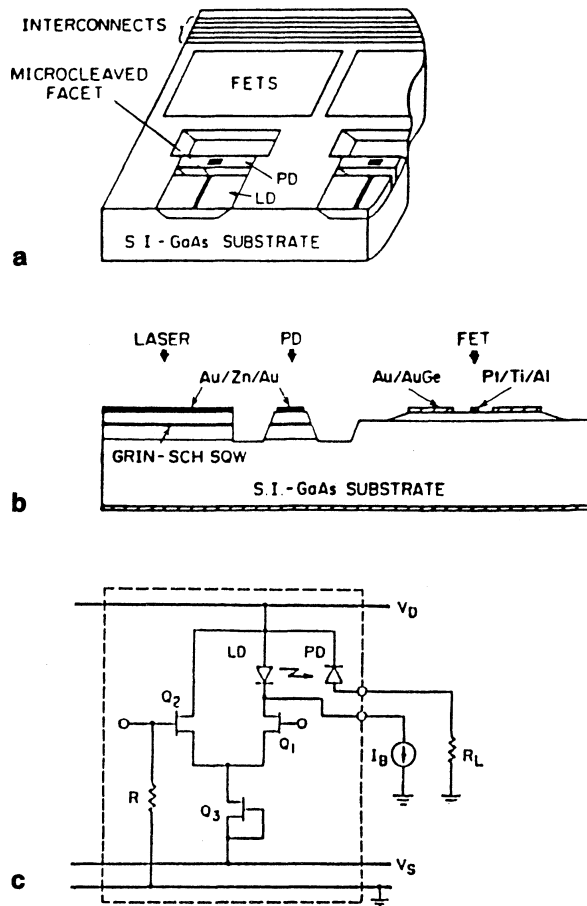


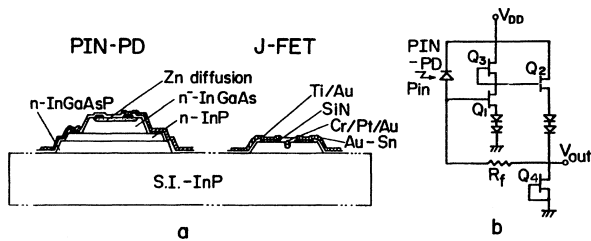
Fig. 20.10 a,b,c Schematic of four-channel OEIC transmitter **a** Over-all view showing the layout, **b** Cross-section along the laser cavity showing the device structure, **c** Circuit diagram of OEIC transmitter. The *dashed line* shows the part of monolithic integration for a single channel

circuits consist of lattice-matched, diffused-junction InGaAs-channel JFETs. Laser modulation at 155 Mbit/s has been achieved.

20.2.2 An OEIC Receiver

The detection and amplification functions of a receiver can also be implemented in OEIC form. Figure 20.11 shows a typical OEIC receiver [37]. The circuit features a p-i-n photodiode detector and Schottky-barrier gate FET amplifier monolithically integrated on a semi-insulating InP substrate. It is designed to operate with a 5 volt

Fig. 20.11 a,b OEIC photoreceiver a. Cross section of circuit chip; b. Circuit diagram [37]



power supply, which simplifies its interconnection with standard 5 volt logic IC's. The circuit has a 3 dB bandwidth of 240 MHz, with a 965Ω transimpedance.

The increased speed of OEIC's as compared to that of discrete element circuits makes them attractive for use in lightwave communication systems, signal processing and sensing applications. Data rates in excess of 40 Gb/s have been achieved in an InP-based OEIC receiver that incorporated a waveguide-integrated photodiode and a distributed amplifier that contained 4 high-electron-mobility transistors (HEMTs) [38]. Optical transceivers that combine both the transmitter and receiver functions also can be made in OEIC form [39–41].

Overall data rates of 100 Gb/s have been achieved in OEIC transceivers. For example, Kish et al. [41] have produced a monolithically integrated chip in InP that features 10 separate transceivers, each operating at a 10 Gb/s data rate. Their outputs are dense-wavelength-division-multiplexed (DWDM) onto a single optical fiber.

20.2.3 An OEIC Phased-Array Antenna Driver

Phased-array antennas have been used for many years in microwave applications in which a scanning microwave beam is required, but a moving antenna structure is impractical [42]. For example, the antenna for a RADAR transmitter in a supersonic aircraft can not be effectively scanned mechanically at a rapid enough rate. In this case, an electronically scanned phased-array antenna is used, consisting of a relatively large number of emitting antenna elements spaced many wavelengths apart, usually along the wings of the aircraft. If the relative phases of the waves transmitted by the various antenna elements are properly adjusted, a scanning microwave beam can be produced. To maintain phase coherence a frequency reference is provided by a stable master oscillator. This reference signal must be properly phase shifted and conveyed to each of the transmitting elements. If metallic microwave waveguide or coaxial cable is used to transport this signal, a great deal of undesirable weight is added to the aircraft. Obviously, this weight can be eliminated if the phase control signals are converted to optical signals and are distributed to the microwave emitters via optical fibers [43].

An OEIC which generates such phase control signals is shown in Fig. 20.12 [44]. The phase control signals are generated in a GaAs monolithic microwave integrated circuit (MMIC) with an integrated laser and driver circuit. These signals are then

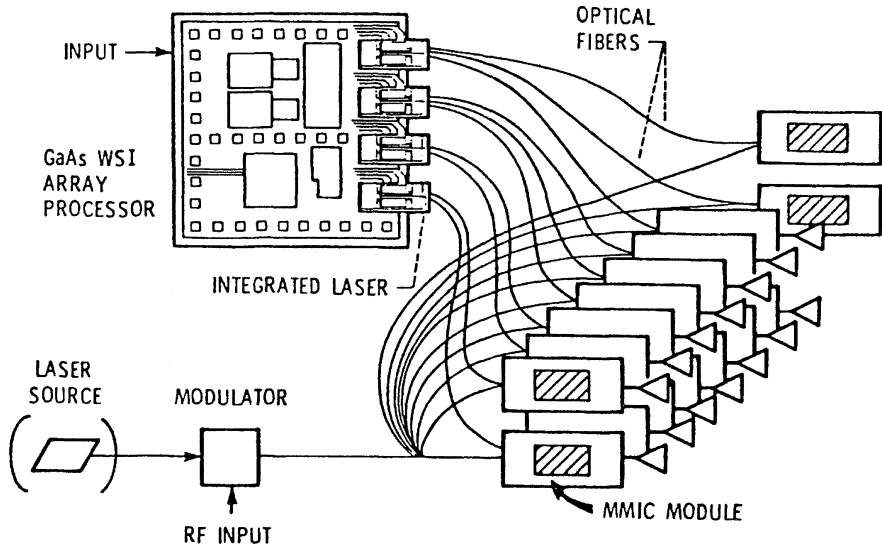


Fig. 20.12 OEIC phased array antenna driver [44]

carried by optical fibers to the microwave generating MMIC modules which are the antenna elements. In the system shown in Fig. 20.12, which was designed for a data transmission application rather than RADAR, an information signal produced by modulating a laser was also carried to all of the antenna elements by optical fiber links.

20.3 Devices and Systems for Telecommunications

While optical integrated circuits are mostly emerging from the laboratory to become commercial products, optical fibers have already found widespread use in telecommunication systems. Almost from its beginning, the use of fiber waveguides in telecommunication systems has been an international phenomenon. Fiber links have been used in many countries to transmit audio and video signals, as well as digital data. There are presently so many examples of fiber telecommunication systems that have either been already implemented or are in the final planning stage that it is impractical to mention all of them in this chapter. Consequently, only a number of representative systems will be considered.

20.3.1 Trends in Optical Telecommunications

Over the past twenty-five years there has been remarkable improvement in the capabilities of optical fiber communications systems. The systems implemented before

5.5 Guided Wave Devices

- Guided wave components are required for routing optical signals on a chip and also for the functions of directional coupling, filtering and modulation.

5.5.1 Waveguides and couplers

- Waveguide is a region of dielectric through which light is propagated, surrounded by dielectric regions or air having a smaller dielectric constant.

Techniques for Fabricating Waveguides:

- To form a guide, varying refractive index regions to be created.
- By introducing free carriers is the simplest technique of defining a guiding region, because in a semiconductor material with a large density of free carriers lowered the refractive index. The lowering of the refractive index due to free carriers is expressed by

$$\Delta n_r = \frac{n\lambda_0^2 q^2}{8\lambda^2 \epsilon_0 n_r m^* C^2}$$

Where

$n_r \rightarrow$ refractive index of the undoped semiconductor at a free space wavelength λ_0 .

- This change in refractive index is large enough for light confinement.
- For obtaining single mode guiding and propagation , it is necessary to define the guiding region in the lateral directions also, by causing an index change.
- This is achieved by three ways such as
 - (i) Ridge waveguide
 - (ii) Buried channel guide
 - (iii) Strip-loaded guide.

(i) Ridge waveguide

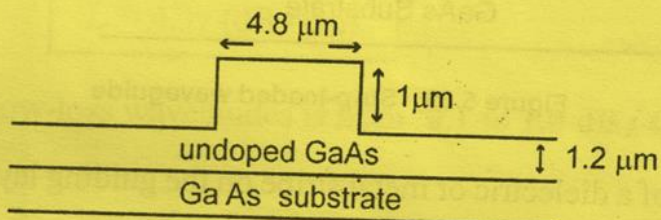


Figure 5.37 Ridge waveguide

- In this, the lateral waveguide dimensions are defined by wet or dry etching or combination of both.
- A dry-etching process such as ion-milling or reactive ion etching provides control, is followed by a wet-etching process, which smoothes the surface.

(ii) Buried channel waveguide:

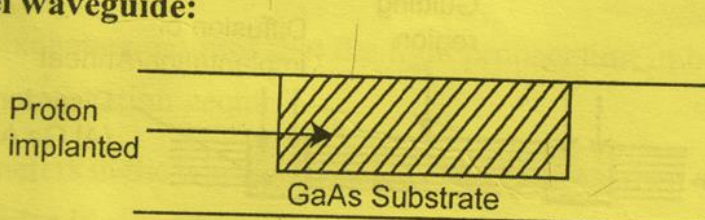


Figure 5.38 Buried channel by implantation

- It can be created by various techniques such as

- (i) Regrowth (simplest method)
- (ii) Diffusion induced disordering .(Novel technique).

- Example of Regrowth is, a GaAs waveguide is grown and defined and a higher-index AlGaAs confining layer is regrown by LPE or MOCVD.
- Selective diffusion technique is a multiquantum well guiding layer is first grown epitaxially, then it is masked selectively and the regions adjacent to the guiding region are doped by implantation.

(iii) Strip-loaded guide:

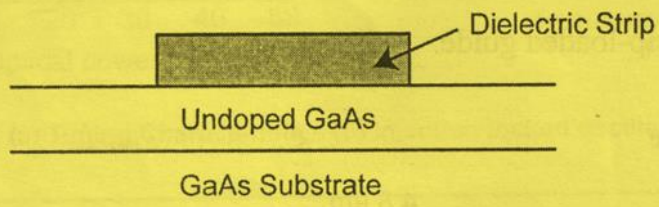


Figure 5.39 Strip-loaded waveguide

- The formation of a dielectric or metal stripe on the guiding layer alters the refractive index of the semiconductor and confines light.
- This is attributed to the spatial variation of the dielectric constant generated by stresses originating in the dielectric or metal stripe.
- The strain, fields in the semiconductor, below the stripe, penetrates to a depth of $2\text{-}3\mu\text{m}$ and therefore, it is suitable for guiding.

(iv) Disordered MQW:

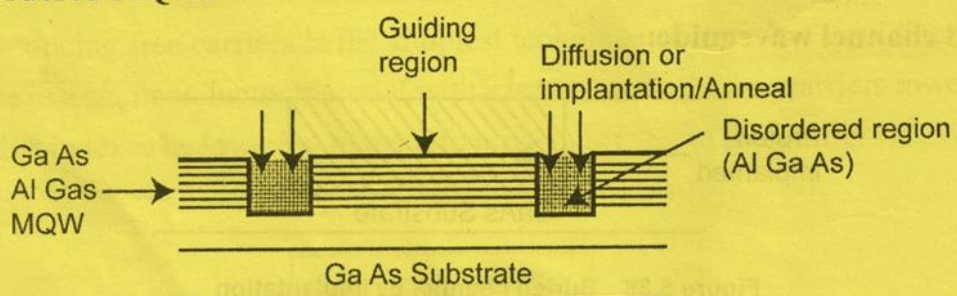


Figure 5.40 Disordered MQW

5.5.1.a Low-Loss waveguides:

- If the guides are made of high-quality, defect free epitaxial layers, then the major sources of loss are surface scattering and absorption.

- Therefore, etching and formation technique become critical in the fabrication of low-loss waveguides.
- Figure of merit is its loss coefficient (γ), which determines the insertion loss of a waveguide, is mainly determined by free-carrier absorption.
- Therefore, material quality and processing become important in determining loss coefficient (γ).
- Transmission of optical power in the guide is given by

$$P(z) = P(0) e^{-\gamma z}$$

from which the guide loss is given by

$$L = 4.3\gamma \text{ (dB / cm)}$$

- The range of Low-loss waveguides is from '**0.1 to 1.0 dB / Cm**'.

5.5.1.b Couplers

- The guided wave integrated optical circuit element is called directional coupler.
- Directional coupler is used for transferring optical energy from one wave guide to another (or) from one region of an OEIC chip to another.
- It consists of two parallel waveguides between which the transfer of optical energy occurs due to the overlapping of waveguide modes.
- This energy exchange requires that the light propagating in both guides have same velocity and propagation vector.
- If these parameters in the two channels are exactly same, then the power propagating in the two guides is given by

$$P_1(z) = \cos^2(Kz) e^{-\gamma z}$$

$$P_2(z) = \sin^2(Kz) e^{-\gamma z}$$

Where

$Z \rightarrow$ direction of propagation

$K \rightarrow$ coupling constant

Coupling constant (K) is given by

$$K = \frac{2\beta_y^2 b e^{-bd}}{\beta_z w (\beta_y^2 + \beta_z^2)}$$

Where

$b \rightarrow$ extinction coefficient

$d \rightarrow$ separation between the guides

$w \rightarrow$ width of each guide

β_y & $\beta_z \rightarrow$ mode propagation constants in the transverse and propagation directions respectively.

- ‘Coupling length (l_c)’ of a directional coupler is defined as the length at which the total transfer of power takes place is given by

$$l_c = \left(m + \frac{1}{2} \right) \frac{\pi}{k}, m = 0, 1, 2, \dots$$

- But in real couplers, the two guides may not be same and hence the propagation constants may differ by a small amount $\Delta\beta_z$.

The coupling constant for real couplers is given by

$$K_r^2 = K^2 + \left(\frac{\Delta\beta_z}{2} \right)^2$$

Dual-Channel Coupler

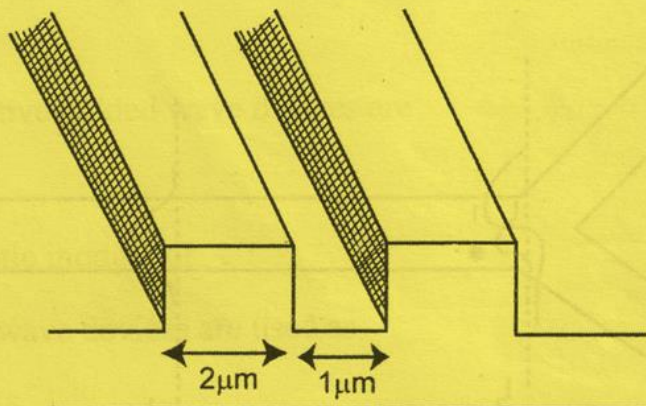


Figure 5.41 Ga As Dual channel single mode ridge waveguide coupler

- Curved sections of guides are important elements of integrated optics.
- Sharp bends constitute a large radiation loss.
- For the bends to loss-free, the radius of curvature at the bend must be larger than ' λ ', the wavelength of light propagating in guide.

5.5.1.c Branching Networks

- ‘Branching networks’ divide optical power among two or more outputs or combine power from two or more inputs.
- The parameters of branching networks are
 - (i) ‘Power division ratio’ – reflects the loss of input power at the output ports.
 - (ii) ‘Excess or insertion loss’ – reflects the loss of input power due to material losses
- Commonly used Branching Network is the waveguide ‘Y’ structure. It can be used as a symmetric power divider or combiner shown in Figure 5.42.

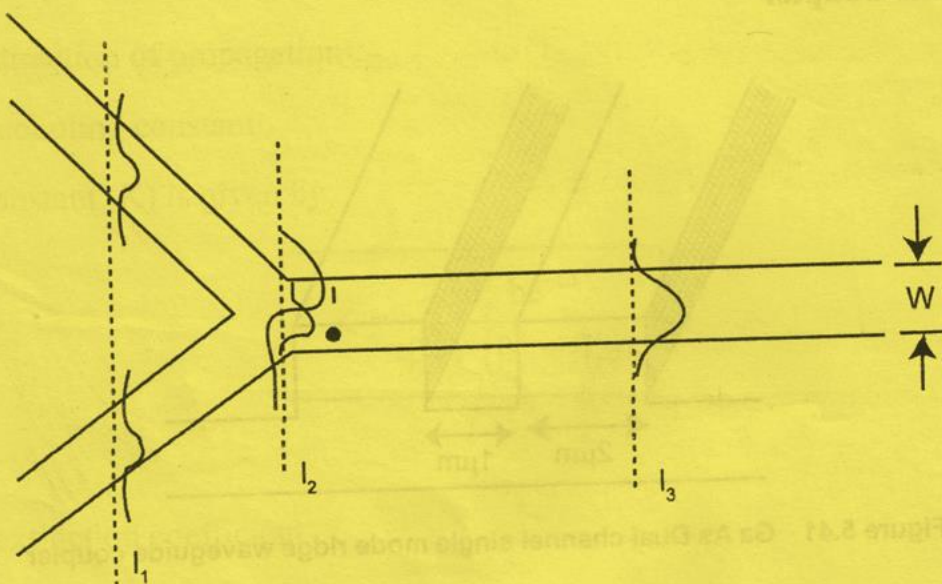


Figure 5.42 Symmetric waveguide Y-Combiner

- The modes at various points of propagation are also illustrated. At point ' l_1 ', the two arms are uncoupled and behave as independent single mode guides, supporting the lower order mode. Near the taper, the structure transitions from a single waveguide of width $2W$ (at l_2) to a waveguide of width W .
- At ' l_2 ', both the symmetric and antisymmetric modes are supported. As these propagate towards point l_3 , the antisymmetric mode is cut off and its energy is radiated into the substrate.
- At ' l_3 ' singlemode characteristics are again restored. For equal input intensities in the two arms, the Y combiner essentially behaves like 3-dB directional couplers.

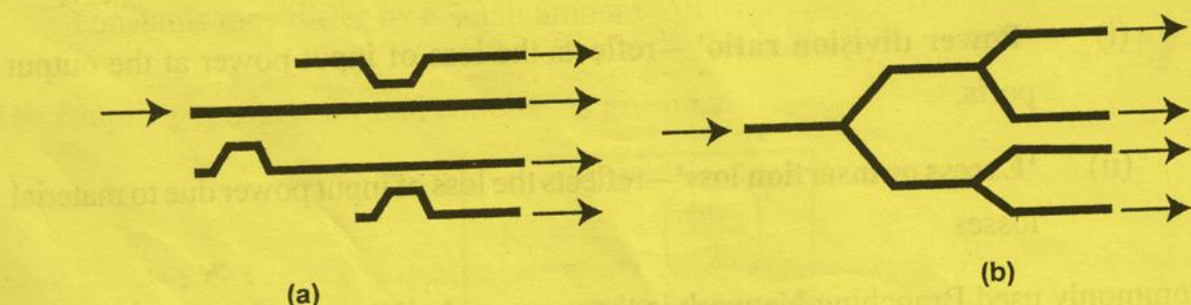


Figure 5.43 (a) Power splitters based on directional coupler
 (b) Power splitter based on Y structure

5.5.2. Active Guided Wave Devices

- Active guided wave components can be integrated in OEICs with active optoelectronic devices.
- Examples of active guided wave devices are
 1. Laser
 2. Electro optic modulator
- Active Guided wave devices are used as
 1. Modulators
 2. Interferometers and
 3. Filters

5.5.2.a Mach-Zehnder Interferometer

- A simple guided wave modulation/switching device based on the electro-optic effect is the mach-zehnder interferometer.

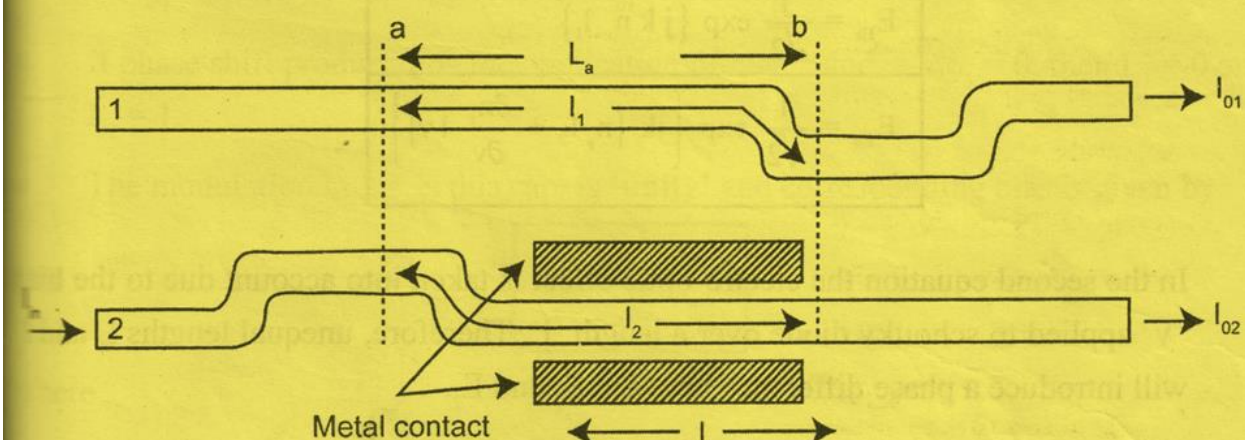


Figure 5.44 Guided wave Mach-Zehnder interferometer

- Figure 5.44 shows the schematic diagram of guided wave mach-zehnder interferometer with input and output 3-dB couplers.
- The incoming optical beam is split equally between the two branches of the input coupler.

- Then recombined at the coupler at the other end.
- To reduce bend losses, we gently care taken in materials growth and processing.
- With no applied bias to the schottky diode, the phase shift in the two arms is equals and at the output coupler the two wave interfere constructively and all the power appears at the output.
- To analyze the switching characteristics of a device, assume the electric field of the input to one arms has unity amplitude and zero phase. According to coupling mode therefore, the fields at point 'a' are given by

$$E_{1a} = 0 + j \sin \frac{\pi}{4} = \frac{j}{\sqrt{2}}$$

$$E_{2a} = 0 + \cos \frac{\pi}{4} = \frac{1}{\sqrt{2}}$$

- At point 'b', the field is phase shifted due to propagation over the length L_a and

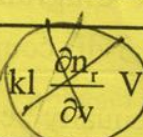
$$E_{1b} = \frac{j}{\sqrt{2}} \exp \{j k n_r l_1\}$$

$$E_{2b} = \frac{1}{\sqrt{2}} \exp \left\{ jk \left\{ n_r l_2 + \frac{\partial n_r}{\partial v} l v \right\} \right\}$$

- In the second equation the electro-optic effect is taken into account due to the bias 'V' applied to schottky diode over a length 'l'. Therefore, unequal lengths l_1 and l_2 will introduce a phase difference between E_1 and E_2 .

$$\Delta\phi_l = k n_r (l_2 - l_1)$$

While the electro-optic effect introduces an additional phase shift.

$$\nabla \phi_{EO} = kl \frac{\partial n_r}{\partial v} V = \frac{\pi l}{\lambda d} n_{r0}^3 r_{ij}^l V$$


Where

$d \rightarrow$ thickness of the wave guide.

- The output coupler recombines the field E_{1b} and E_{2b} to give the field output of arm 1 as

$$E_{01} = -\frac{j}{2} \exp(jk n_r l_1) [1 + \exp\{j(\Delta\phi_1 + \Delta\phi_{E0})\}]$$

- The output intensity from the arm, is obtained by taking square of the magnitude of the field.

$$I_{01} = \frac{1}{2} [1 + \cos(\Delta\phi_1 + \Delta\phi_{E0})]$$

- Similarly, we can obtain the output from arm 2

$$I_{02} = \frac{1}{2} [1 - \cos(\Delta\phi_1 + \Delta\phi_{E0})]$$

- If the device is loss less, then the sum of I_{01} and I_{02} is equal to the input intensity.
- The $l_1 = l_2$ and no bias applied, then $I_{01} = 1$ and $I_{02} = .0$
- If phase shift produced by the application of bias π and $= \Delta\phi_1 = 0$, then $I_{01} = 0$ and $I_{02} = 1$.
- The modulation index in this care is '**unity**' and corresponding bias is given by

$$V_\pi = \frac{\lambda d}{\ln_{r_0}^3 r_{ij}^1}$$

Where

- Subscript π denotes a '**half wave phase shift**' and V_π is also called '**half wave voltage**'.